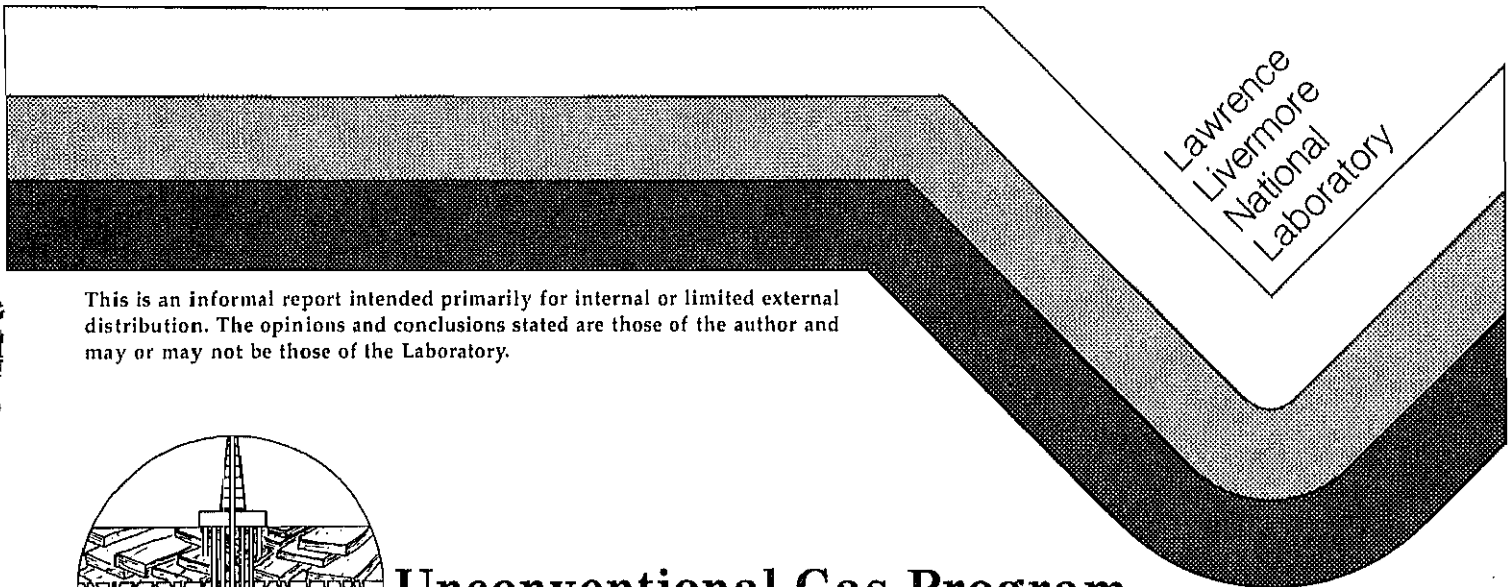


ULTRASONIC VELOCITIES AND DYNAMIC ELASTIC MODULI OF MESAVERDE ROCKS

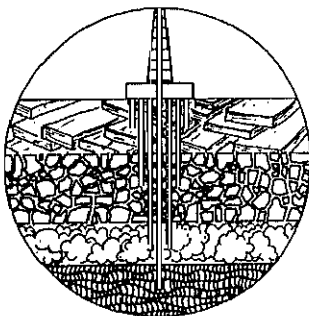
Wunan Lin

Prepared for
Morgantown Energy Technology Center
Morgantown, WV

March, 1985



This is an informal report intended primarily for internal or limited external distribution. The opinions and conclusions stated are those of the author and may or may not be those of the Laboratory.



Unconventional Gas Program

Western Gas Sands Research

DISCLAIMER

This document was prepared as an account of work sponsored by an agency of the United States Government. Neither the United States Government nor the University of California nor any of their employees, makes any warranty, express or implied, or assumes any legal liability or responsibility for the accuracy, completeness, or usefulness of any information, apparatus, product, or process disclosed, or represents that its use would not infringe privately owned rights. Reference herein to any specific commercial products, process, or service by trade name, trademark, manufacturer, or otherwise, does not necessarily constitute or imply its endorsement, recommendation, or favoring by the United States Government or the University of California. The views and opinions of authors expressed herein do not necessarily state or reflect those of the United States Government or the University of California, and shall not be used for advertising or product endorsement purposes.

Printed in the United States of America
Available from
National Technical Information Service
U.S. Department of Commerce
5285 Port Royal Road
Springfield, VA 22161
Price: Printed Copy \$; Microfiche \$4.50

<u>Page Range</u>	<u>Domestic Price</u>	<u>Page Range</u>	<u>Domestic Price</u>
001-025	\$ 7.00	326-350	\$ 26.50
026-050	8.50	351-375	28.00
051-075	10.00	376-400	29.50
076-100	11.50	401-426	31.00
101-125	13.00	427-450	32.50
126-150	14.50	451-475	34.00
151-175	16.00	476-500	35.50
176-200	17.50	501-525	37.00
201-225	19.00	526-550	38.50
226-250	20.50	551-575	40.00
251-275	22.00	576-600	41.50
276-300	23.50	601-up ¹	
301-325	25.00		

¹Add 1.50 for each additional 25 page increment, or portion thereof from 601 pages up.

INDEX

ABSTRACT	ii
1. INTRODUCTION	1
2. ROCK DESCRIPTION AND SAMPLE PREPARATION	3
2.1 Rock Description	3
2.2 Sample Preparation	6
3. EXPERIMENTAL PROCEDURES	8
4. RESULTS AND DISCUSSIONS	10
4.1 Ultrasonic Velocities	10
4.2 Dynamic Elastic Moduli	12
4.3 Comparison of Static Elastic Moduli and Dynamic Elastic Moduli	13
4.4 Comparison of In Situ Velocities and Laboratory Velocities	16
5. SUMMARY	18
6. REFERENCES	19
7. ACKNOWLEDGMENTS	21
8. APPENDIX A	22
9. APPENDIX B	43

ABSTRACT

Ultrasonic P-wave and S-wave velocities were measured in Mesaverde sandstones and shales as function of confining pressure to 650 MPa, in six directions concurrently. The samples came from five wells in Colorado and Wyoming. The Mesaverde sandstones are quite isotropic; the shales are transversely isotropic with the direction perpendicular to bedding being the slow direction for wave propagation. The anisotropy of the shale is up to 13% for P-waves and 17% for S-waves.

The velocity-pressure behavior of these rocks reveals microscopic structural differences between the sandstones and shales. The sandstones contain microcracks that are closed at moderate pressures (less than 100 MPa). The shales do not have the obvious discontinuity in the pressure/velocity record that can be attributed to the microcrack closing. In situ velocities obtained from the well logs of four of the five wells are compatible with the laboratory determined velocities.

Dynamic elastic moduli of the rocks at the overburden pressures (8 to 98 MPa) were calculated from the wave velocities and bulk density. They were compared to static laboratory moduli obtained on corresponding rocks from the same wells. The dynamic moduli are greater than the static elastic moduli by 50 to as much as 600%. The dynamic Poisson's ratios are much smaller than the static ones. Some of the calculated dynamic Poisson's ratios have small negative values.

This work highlights the need for a better definition of which mechanical properties tests are relevant to the design of hydrofracturing in tight gas formations.

1. INTRODUCTION

It is estimated that low-permeability western gas reservoirs in the U.S. contain large quantities of natural gas. In order to recover these resources economically, the region around a production well must be stimulated to induce a more rapid flow of the natural gas into the well bore. Currently, the most promising techniques for stimulating low-permeability gas reservoirs is with fluids under pressure.

The goal of the research in support of the DOE's Western Gas Sands Subprogram at the Lawrence Livermore National Laboratory (LLNL) is to obtain a more detailed understanding of stimulation processes (1). Current methods for predicting intensity, geometry, and extent of fracturing resulting from hydraulic stimulation require certain equation-of-state (EOS) measurements as input data to the calculation codes. To that end, we have measured the mechanical properties of Mesaverde shale and sandstone, and those of sandstones and siltstones from the Multiwell (MWX) field test site, in static laboratory tests (2,3). We are now complementing these earlier studies by measuring ultrasonic velocities of P and S-waves in Mesaverde sandstone and shale samples obtained at various depths from five vertical boreholes drilled in Colorado and Wyoming.

This study is designed to estimate the dynamic elastic moduli and Poisson's ratios of the Mesaverde rocks as functions of confining pressure, at room temperature, and to compare those values to the static values reported in reference (2) for corresponding rocks from the same wells.

Laboratory measured physical properties of rock are necessary input parameters to models that analyze and/or predict the response of rock masses to certain engineered or natural disturbances. The laboratory samples are usually homogeneous and small whereas the rock mass is large and contains both

discontinuities and inhomogeneities. However, the laboratory test results on small and intact samples can still provide useful, information if the discontinuities can be characterized independently. Then, a composite picture of the rock mass behavior can be assembled based on intact material plus discontinuity properties.

Elastic moduli of rock are frequently used in the study of geomechanical problems. Ultrasonic velocities have been used to estimate these moduli (4). Ultrasonic velocity measurements are important for another reason: seismic refraction and reflection are common tools for resource exploration and crustal studies. Although the field seismic velocities can be different from the laboratory measured ultrasonic velocities near the surface where fault, joints, and other discontinuities are abundant, the laboratory values have been shown to match field measurements at depths where major fractures are closed (5-7).

For a transversely isotropic rock, as a sedimentary rock is most likely to be, simultaneous measurements of velocities in six directions enable calculating the complete tensor of elastic moduli if the bulk density is also known. The velocities were measured as function of confining pressure so that an extrapolation could be done to estimate the moduli at depth.

2. ROCK DESCRIPTION AND SAMPLE PREPARATION

2.1 Rock Description

The samples used in this study were from the same source as those used in the measurements of mechanical properties (2). Table 1 lists the well locations and the depth at which the core samples were obtained. The rocks are grouped according to well locations. The rock types along with their group numbers will be used throughout this report for ease of identification.

The cores contain alternating sections of sandstone and shale. Generally, bedding planes in the pure sandstone and shale sections are not easily determined by visual inspection. We assume that the bedding plane is parallel to the interface between the sandstone and shale sections and is usually horizontal. Table 2 summarizes the grain size, color, and dry-bulk and grain density of the rock types. The sandstone sections of the cores are usually quite homogeneous. On the other hand, some of the shale sections, for instance Shale 1 and Shale 2, show variations in color and dry-bulk and grain densities. No grain size data are available for the shale samples.

The mineral composition of the rocks listed in Table 3 was determined by x-ray analysis. This table also shows that the quartz content of the sandstone increases but varies with depth. Shales 4 and 5 contain almost as much quartz as the corresponding sandstones. At a depth less than 1958 m, the shale usually contains larger amounts of clay minerals, such as illite, kaolinite, montmorillonite, etc., than the sandstone. The rocks from deeper than 1958 m contain no more than a trace amount of clay minerals.

Table 1. Location and depth of Mesaverde formation rock samples used in this study.

Rock Type	Group	Well Name	Location	Depth (m)
Sandstone	1	Twin Arrow C&K 4-14	Rio Blanco, CO	352
Shale	1	"	"	350
Sandstone	2	PTS 24-19 Federal	Sublette, WY	1582
Shale	2	"	"	1599
Sandstone	3	PTS 22-12 Federal	Rio Blanco, CO	1958
Shale	3	"	"	1968
Sandstone	4	PTS 3-10-A	Sweetwater, WY	3512
Shale	4	"	"	3511
Sandstone	5	Rainbow Resources	Sweetwater, WY	3805
Shale	5	1-3 Federal	"	3883

Table 2. Grain sizes, colors, and densities of the Mesaverde rocks.

<u>Rock</u>	<u>Grain Size</u>	<u>Color</u>	<u>Dry Bulk Density</u> (Mg/m ³)	<u>Grain Density</u> (Mg/m ³)
Sandstone 1	~ 0.5 mm	beige	2.094 ± 0.011	2.68
Shale 1	Very fine	black grey-grey	2.254 ± 0.056	2.35
Sandstone 2	~ 0.1-0.2mm	grey	2.546 ± 0.006	2.73
Shale 2	Very fine	dark grey	2.505 ± 0.012	2.64
Sandstone 3	~ 0.1-0.2mm	light grey	2.345 ± 0.011	2.69
Shale 3	Very fine	grey	2.660 ± 0.007	2.69
Sandstone 4	~ 0.1	light grey	2.536 ± 0.004	2.71
Shale 4	Very fine	dark grey	2.610 ± 0.012	2.89
Sandstone 5	0.2-0.3 mm	light grey	2.407 ± 0.016	2.87
Shale 5	Very fine	grey to dark grey	2.516 ± 0.016	2.92

Table 3. Mineral composition of Mesaverde rocks determined by x-ray analysis.

Rock Type	Mineral Composition
Sandstone 1	Quartz (85%), illite-muscovite (5%), kaolinite-nacrite (5%), bytownite or anorthite (5%), montmorillonite (trace)
Shale 1	Quartz (75%), illite-muscovite (15%), kaolinite-nacrite (5%), bytownite or anorthite (5%), montmorillonite (trace)
Sandstone 2	Quartz (80%), kaolinite-nacrite (13%), illite-muscovity (5%), montmorillonite (trace)
Shale 2	Quartz (65%), illite-muscovite (15%), kaolinite-nacrite (10%), dolomite (5%), calcite (1-5%), montmorillonite (trace)
Sandstone 3	Quartz (95%), caccite (trace), plagioclase-oligoclase (trace), kaolinite (trace)
Shale 3	Quartz (85%), calcite (10%), plagioclase-oligoclase (trace), kaolinite (trace)
Sandstone 4	Quartz (~ 100%), plagioclase - oligoclase (trace)
Shale 4	Quartz (95%), plagioclase - oligoclase (trace), kaolinite (trace)
Sandstone 5	Quartz (~ 100%)
Shale 5	Quartz (~ 100%), calcite (trace), kaolinite (trace)

2.2 Sample Preparation

The traditional method of determining ultrasonic velocity of anisotropic material is to core small cylindrical samples in the directions with the most anisotropic characteristics (8). The major disadvantage of the traditional approach is the introduction of sample variation into the measured value. In this study we prepared the sample in a way that made simultaneous measurements of velocities in six directions possible.

The core sections were cut into cubes with dimensions ranging from 3.5 cm to 5.0 cm, dependent on the diameter of the original core section. One of the cubic surfaces was coincident with the bedding plane of the rock. It was designated as "A". The principal axis AA of the cube (in Miller indicies designated 001) is then perpendicular to bedding. The directions B and C (010 and 100) are arbitrary. The edges of the cubes (110) were then cut off to form a flat surface diagonal to the axes of the cube with widths ranging from 1.0 to 1.5 cm. Figure 1 shows one example of the cube SS3 equipped with ultrasonic transducers. The surface A in Figure 1 is that with numbers on it.

The sample was then dried at a temperature of about 30°C in a vacuum oven to remove the water used in cutting until its weight remained unchanged for at least one day. The dry bulk density and grain density listed in Table 2 were determined from cylindrical samples cored from the same core section (2). A layer of silver paint no more than 0.03 mm thick was then coated on the entire surface of the cubic sample to form a conductive ground for the ultrasonic transducers.

Three ultrasonic transducers, one P-wave and two S-wave, were mounted on each principal face of the sample. One P-wave transducer was mounted on each face of one pair of the diagonal faces (Figure 1). The transducers were of PZT with a natural frequency of 1 MHz. The two S-wave transducers on each principal face were oriented in such a way that the polarizations of the S-waves were parallel to one of the principal axis of the sample and orthogonal to each other. The sample with the electrical wires attaching to the transducers was then encapsulated in Scotch cast resin (8).

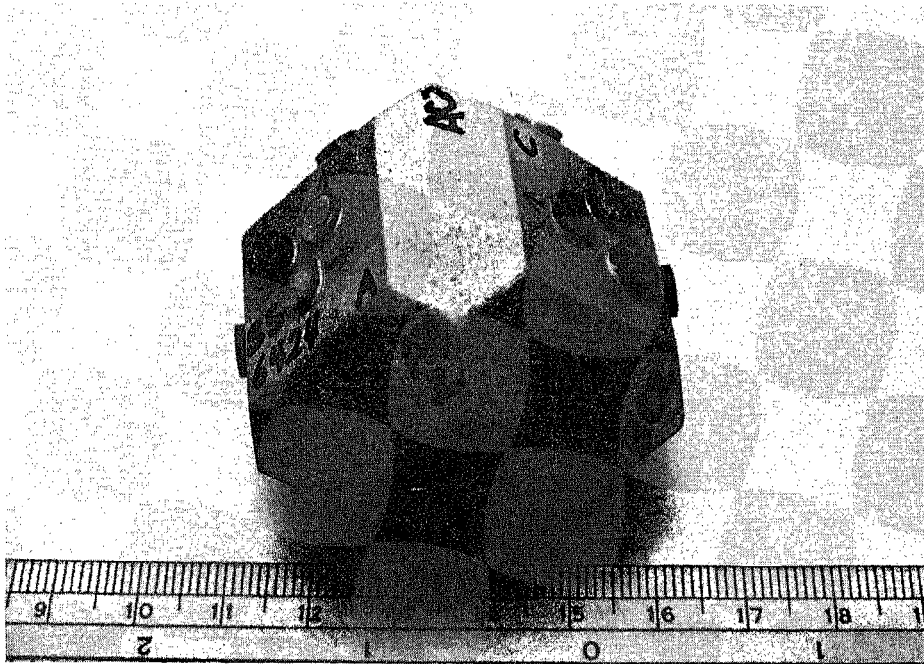


Figure 1. A SS3 sample with transducers. The three principal faces are A, B, and C. The diagonal faces AB, AC, and BC are between the corresponding two principal faces. The scale is in cm.

3. EXPERIMENTAL PROCEDURES

In our pressure system we used Octoil as the pressure medium. The confining pressure was generated by an air-oil Haskel pump driving an intensifier with a 10 to 1 ratio. The confining pressure was read from a Heise gage with a smallest division representing 0.5 MPa.

The traditional direct transmission method was used to measure travel time of ultrasonic waves in the sample. The method has been well described (8). In this study, the travel time was measured between one pair of the transducers at a time. There are twelve travel times to be measured at every pressure step. The twelve travel times are PA, PB, PC, PAB, PAC, and PBC for P-waves propagating in the direction perpendicular to faces A, B, C, AB, AC, and BC; and SAB, SAC, SBA, SBC, SCA, and SCB for S-waves propagating perpendicular to the A, B, and C faces and polarized in the direction perpendicular to B(SAB), C(SAC) and so on. The measurements were repeated when the confining pressure was changed to the next level. The travel times measured in this way avoided interference from waves propagating in other directions. The travel times were measured to a confining pressure of 400 to 500 MPa for most of the samples. For SS1 the travel time was measured to 650 MPa.

The travel times were then corrected for the system delay time of the electronics (including the transducers) and the shortening of wave path due to hydrostatic compression. The system delay time for the P-wave and S-wave were 0.32 μ s and 1.68 μ s, respectively. To calculate the wave path shortening, we used the previously determined hydrostatic compressibility of these rocks

in the directions perpendicular and parallel to bedding (2). We assumed that the samples were transversely isotropic. Based on our measured travel times and compressibility, this assumption was very good.

It is well known that when a wave propagates inclined to a principal axis in an anisotropic medium the direction of particle motion may deviate from the direction of wave propagation (9,10). For the PAB, PAC and PBC waves we calculated the angle of deviation between the direction of wave propagation and particle motion using the formula by Fisher and McSkimin (11). The deviation angles all were within 1 to 2° at pressures corresponding to the overburden pressure (Ref. 2) or greater. The largest deviation angle occurred at 0.1 MPa pressure (room conditions). In this case it was 9.12° for sample SS4. This angle corresponds to a length difference in traveling path of about 1%.

The factors that contributed to the experimental uncertainty of the ultrasonic velocity measurements were determination of wave arrival, measurement of travel time, measurement of wave path distance, and the measurement of confining pressure. The total uncertainty for determining P-wave velocity at pressures was about 2 to 3%. For the determination of S-wave velocity, the total uncertainty was about 4 to 6%.

4. RESULTS AND DISCUSSION

4.1 Ultrasonic Velocities

The ultrasonic velocities in the Mesaverde rocks were calculated from the corrected travel time data by dividing the travel path length by the travel time. The velocities are plotted as function of confining pressure in Figs. 2 to 11 (Appendix A). In these figures, the upper group of curves is the P-wave velocity, the lower group is the S-wave velocity.

The velocity vs. pressure plots of the sandstones are quite different than that of the shales. For the sandstones (Figs. 2, 4, 6, 8, and 10) both P-wave and S-wave velocities have a rapid increase with increasing pressure at pressures below 100 GPa. Then at higher pressures the velocity increases are much gentler. For most of the shale samples (Figs. 5, 7, 9, and 11) the abrupt change in $\frac{\partial v}{\partial p}$ is not as evident. The rapid increase of velocity with pressure at low pressures has been attributed to the closing up of microcracks in the sample under pressure (5). One exception among the shales is SH1 (Fig. 3) where the velocities show similar behavior as the sandstone, although the $\frac{\partial v}{\partial p}$ at low pressures is much smaller than that of SS1 (Fig. 2). The behavior between the sandstones and the shales indicates some basic difference in microscopic texture in these two rocks. The different behavior of SH1 compared with other shales may indicate that the existence of microcracks in shale is dependent on the depth of burial because it is the shallowest. It is also the least dense shale.

Figures 2 through 11 show that all of the velocity vs. pressure curves in either the P-wave or S-wave group are parallel to each other. Therefore, even though some rocks have velocity anisotropy (see below), the velocity in different directions varies with confining pressure in about the same way for each rock.

For comparison we list the wave velocities in these rocks at their corresponding overburden pressure (P_o) in Table 4. In the case of SS1 and SH1 the core section was not large enough to prepare a sample big enough for all of the measurements. But the values shown in Table 4 represent the velocity ranges for these two rocks. For SH4 the signal of SBA and SCB were not good enough for accurate measurement.

Generally speaking the Mesaverde sandstones are fairly isotropic. Except for the P-wave velocities measured for SS1 and SS2, the anisotropy of the sandstones are no more than 5%. Even for SS1 and SS2 the anisotropy of P-wave velocity is no more than 7%. On the other hand, most of the shales show quite strong anisotropy in both P-wave and S-wave velocities. The greatest anisotropy in velocity is seen in SH4 which is 13% for the P-wave and 17% for the S-wave.

It also shown in Table 4 that the velocities of the shales are very similar to that of a transversely isotropic material. When the sandstones show some degree of anisotropy they are also transversely isotropic.

The slowest direction of the ultrasonic waves in most of the Mesaverde rocks are perpendicular to bedding. One exception is SS5 where one of the directions parallel to bedding is as slow as the directions perpendicular to bedding. However, the difference is only slightly greater than experimental uncertainty.

Table 4. Ultrasonic velocities along the principal axes of Mesaverde rocks at overburden pressures (P_o).

	SS1	SH1	SS2	SH2	SS3	SH3	SS4	SH4	SS5	SH5
P_o (MPa)	8	8	40	40	50	50	90	90	98	98
VPA(km/s)	3.04	3.01	4.08	4.10	4.53	4.85	5.06	4.77	5.18	4.36
VPB(km/s)	3.24	--	4.24	4.48	4.72	5.13	5.21	5.38	5.18	4.78
VPC(km/s)	--	3.33	4.32	4.61	4.70	5.18	5.11	5.33	5.32	4.73
VSAB(km/s)	2.05	2.25	2.94	2.77	3.21	3.16	3.60	3.21	3.85	2.96
VSBA(km/s)	--	--	2.93	3.00	3.14	3.10	3.61	--	3.83	2.92
VSAC(km/s)	--	--	2.98	2.80	3.22	3.16	3.56	3.24	3.74	2.95
VSCA(km/s)	--	--	2.99	2.99	3.23	3.19	3.57	3.42	3.79	2.90
VSCB(km/s)	2.09	2.37	3.00	2.90	3.31	3.27	3.63	--	3.90	3.17

4.2 Dynamic Elastic Moduli

We used the formula suggested by McSkimin (4) to calculate the stiffness coefficients of the Mesaverde rocks as function of confining pressure. As mentioned in Section 2, the frequency of the ultrasonic wave was 1 MHz. The strain applied by the ultrasonic waves was very small, of the order of 10^{-6} , therefore the moduli calculated from the measured ultrasonic wave velocities are elastic moduli. We used a Cartesian coordinate with Z-axis perpendicular to bedding, i.e., perpendicular to face A. The other orthogonal axes x and y were chosen arbitrarily. We set $x=B$ and $y=C$. The five independent stiffness coefficients are then C_{11} ($= C_{22}$), C_{33} , C_{44} ($= C_{55}$), C_{66} , and C_{13} .

The bulk density as a function of confining pressure, was calculated from the dry bulk density at 0.1 MPa and the bulk compressibility of the rocks reported previously (2).

Figures 12 through 21 show the stiffness coefficients of these rocks as functions of confining pressure (Appendix A). In these figures, curve 1 is C_{11} ; curve 2 is C_{33} ; curve 3 is C_{44} ; curve 4 is C_{66} ; and curve 5 is C_{13} . As expected, the stiffness coefficients behave very similarly to the ultrasonic velocities -- the sandstones are fairly isotropic, and the shales are transversely isotropic with respect to the bedding plane.

The relative values of the diagonal member of the stiffness (C_{11} , C_{33} , C_{44} and C_{66}) between the sandstone and the shale vary with depth of sample origin. The stiffness coefficients of SS1 are smaller than SH1; the stiffness coefficients of SS5 are greater than that of SH5.

In some cases the value of C_{13} becomes negative. This was shown to exist in orthotropic composites. The stiffness coefficients of the rocks passed the stability tests suggested by Alers and Neighbors (12).

4.3 Comparison of Static Elastic Moduli and Dynamic Elastic Moduli

For the purpose of comparing with the static elastic properties, the dynamic Young's moduli (E_{xD} and E_{zD}), dynamic shear moduli (G_{xyD} and G_{xzD}), and dynamic Poisson's ratios (ν_{xyD} and ν_{xzD}) were calculated from the dynamic stiffness coefficients (C_{11} , C_{13} etc.). Note, however, that the static G_{xz} was not measured, as explained in reference (2). In a transversely isotropic material the correspondence between stiffness coefficients and elastic moduli and Poisson's ratios is:

$$\begin{bmatrix} C_{11} & (C_{11}-2C_{66}) & C_{13} & 0 & 0 & 0 \\ (C_{11}-2C_{66}) & C_{11} & C_{13} & 0 & 0 & 0 \\ C_{13} & C_{13} & C_{33} & 0 & 0 & 0 \\ 0 & 0 & 0 & C_{44} & 0 & 0 \\ 0 & 0 & 0 & 0 & C_{44} & 0 \\ 0 & 0 & 0 & 0 & 0 & C_{66} \end{bmatrix}^{-1} \equiv \begin{bmatrix} \frac{1}{E_x} & -\frac{\nu_{xy}}{E_x} & -\frac{\nu_{xz}}{E_x} & 0 & 0 & 0 \\ -\frac{\nu_{xy}}{E_x} & \frac{1}{E_x} & -\frac{\nu_{xz}}{E_x} & 0 & 0 & 0 \\ -\frac{\nu_{xz}}{E_z} & -\frac{\nu_{zx}}{E_z} & \frac{1}{E_z} & 0 & 0 & 0 \\ 0 & 0 & 0 & \frac{1}{G_{xz}} & 0 & 0 \\ 0 & 0 & 0 & 0 & \frac{1}{G_{xz}} & 0 \\ 0 & 0 & 0 & 0 & 0 & \frac{1}{G_{xy}} \end{bmatrix}$$

We only compared the dynamic elastic properties and the static elastic properties at the overburden overburden pressure (P_o). Table 5 shows the comparison.

The dynamic moduli are always greater than the static moduli. This has been extensively documented for numerous rock types (13-17), including gas bearing formations (18). However, the amplitude of the difference is quite large for the Mesaverde rocks. For example, in Westerly granite and diabase the dynamic moduli was about 20% greater than the static moduli. In this study the dynamic moduli are greater than the static moduli by up to more than 600%.

Table 5. Dynamic Young's moduli (E_{xD} , E_{zD}), shear modulus (G_{xyD}), and Poisson's ratios (ν_{xyD} , ν_{xzD}) of the Mesaverde rocks compared to the corresponding static moduli (E_{xS} , E_{zS} , G_{xyS}) and Poisson's ratios (ν_{xyS} , ν_{xzS}) from reference (2).

Rocks	P_o (MPa)	$\frac{E_{xD}}{E_{xS}}$ (GPa)	$\frac{E_{zD}}{E_{zS}}$ (GPa)	$\frac{G_{xyD}}{G_{xyS}}$ (GPa)	G_{xzD} (GPa)	$\frac{\nu_{xyD}}{\nu_{xyS}}$	$\frac{\nu_{xzD}}{\nu_{xzS}}$
SS1	8	$\frac{21.46}{--}$	$\frac{19.01}{--}$	$\frac{9.52}{--}$	8.84	$\frac{0.14}{--}$	$\frac{0.09}{--}$
SH1	8	$\frac{24.86}{--}$	$\frac{20.37}{--}$	$\frac{12.67}{--}$	11.38	$\frac{-0.019}{--}$	$\frac{-0.06}{--}$
SS2	40	$\frac{47.62}{10.45}$	$\frac{42.55}{10.3}$	$\frac{23.41}{3.8}$	22.59	$\frac{0.017}{0.37}$	$\frac{-0.007}{0.30}$
SH2	40	$\frac{51.02}{8.14}$	$\frac{42.02}{7.16}$	$\frac{21.08}{3.11}$	19.83	$\frac{0.21}{0.31}$	$\frac{0.06}{0.39}$
SS3	50	$\frac{51.81}{17.07}$	$\frac{48.08}{16.91}$	$\frac{25.83}{6.57}$	24.40	$\frac{0.0031}{0.31}$	$\frac{-0.05}{0.27}$
SH3	50	$\frac{67.57}{--}$	$\frac{60.98}{--}$	$\frac{28.46}{--}$	26.58	$\frac{0.19}{--}$	$\frac{0.12}{--}$
SS4	90	$\frac{66.67}{41.05}$	$\frac{65.36}{42.27}$	$\frac{33.72}{17.18}$	32.35	$\frac{-0.011}{0.20}$	$\frac{-0.004}{0.22}$
SH4	90	$\frac{75.19}{17.86}$	$\frac{58.14}{21.14}$	$\frac{36.79}{6.64}$	27.05	$\frac{0.22}{0.35}$	$\frac{0.09}{0.33}$
SS5	98	$\frac{66.23}{23.36}$	$\frac{60.98}{21.82}$	$\frac{37.02}{9.23}$	36.01	$\frac{-0.11}{0.27}$	$\frac{-0.19}{0.25}$
SH5	98	$\frac{56.50}{10.34}$	$\frac{47.17}{8.86}$	$\frac{25.57}{3.69}$	22.24	$\frac{0.11}{0.33}$	$\frac{0.12}{0.44}$

The difference between dynamic and static moduli has been attributed to the different level of stress applied to the sample in the two methods of measurement (19). In ultrasonic measurements the stress applied to the sample is very small so that no sliding of mineral grains may occur. For the Mesaverde rocks the sliding of mineral grains during the static measurements may have a more profound effect on reducing the moduli values than in the igneous rocks such as granite and diabase (15). The static and dynamic measurements were done on different samples. This may contribute to part of the difference in the results, but not that much.

The dynamic Poisson's ratios are always smaller than the static Poisson's ratios. This was, again, observed before (18). The explanation for this phenomenon is the same as that for the moduli. However, several of the Mesaverde rocks have small negative Poisson's ratios. A negative Poisson's ratio is not physically impossible but it is unusual for rock. It has been noted before that the dynamic Poisson's ratio measurement is intrinsically inaccurate because it involves the difference of two quantities of similar magnitude (19).

4.4 Comparison of In-Situ Velocity and Laboratory Ultrasonic Velocity

In-situ P-wave velocity in rocks from four of the five wells (except the shallowest well, Twin Arrow C & K 4-14) was calculated from the travel time measured by sonic logs. The P-wave velocity is plotted as a function of depth, as shown in Figures 22 to 25 (Appendix B). Also plotted in these figures are the laboratory determined P-wave velocities, perpendicular to bedding, of the Mesaverde sandstone and shale from these wells at the corresponding overburden pressure.

In most of the cases the laboratory measured velocity is greater than the in-situ velocity measured by sonic log. The P-wave velocity of the sandstone from PTS 24-19 well (well #2 in Table 1) falls below the sonic velocity at the same depth. However, generally speaking the laboratory determined velocity is quite compatible with the sonic velocity. Normally one expects the laboratory determined velocity to be greater than the in-situ sonic velocity, because the laboratory sample is homogeneous and intact whereas the region between the transmitter and receiver of a sonic logging tool may contain cracks and joints. Our results indicate that at the depth of sample origin the effect of discontinuities (fractures, joints,...) on the sonic velocity is not significant.

5. SUMMARY

We have measured ultrasonic wave velocities in Mesaverde sandstones and shales in six directions simultaneously as function of confining pressure to 650 MPa, at room temperature. This is consistent with the mechanical properties reported separately on the same rocks. The shales, however, are transversely isotropic with the perpendicular to bedding being the slow direction for wave propagation. The anisotropy of the shales may be as great as 13% in P-wave velocity and 17% in S-wave velocity.

The laboratory determined ultrasonic P-wave velocities perpendicular to bedding of the Mesaverde sandstone and shale are quite compatible with the in situ P-wave velocities at the same depth measured by sonic logging. This indicates that the effect of discontinuities (fractures, joints, etc.) on the in-situ velocity is not significant.

The dynamic elastic moduli and Poisson's ratios of the Mesaverde rocks were calculated. Comparison with the static moduli and Poisson's ratios indicates that the dynamic moduli are greater than the static moduli and the dynamic Poisson's ratios are smaller than the static ones. The differences between the dynamic and static moduli of the Mesaverde rocks are significantly greater than usually reported for other rocks.

This work demonstrates the need for a better definition for which mechanical properties tests are relevant to the design of hydrofracturing in tight gas formations.

6. REFERENCES

1. Heuze, F.E., (1984) "The Western Gas Sands Subprogram at Lawrence Livermore National Laboratory", Lawrence Livermore National Laboratory, UCRL-89890-84, December.
2. Lin, W., (1985) "Strength and Static Elastic Moduli of Mesaverde Rocks", Lawrence Livermore National Laboratory, UCID-20370, March.
3. Lin, W., (1984) "Mechanical Properties of Multiwell MWX-1 Sandstone and Siltstone at High Pressures", Lawrence Livermore National Laboratory, UCRL-53535.
4. McSkimin, H.J., (1964) "Ultrasonic Methods for Measuring the Mechanical Properties of Liquid and Solids", in Physical Acoustics, ed. by W. P. Mason, Vol. I. Part A, pp. 334.
5. Lin, W., and C. Wang, (1980) "P-wave Velocities in Rocks at High Pressure and Temperature and the Constitution of the Central California Crust", Geophys. J. R. Astr. Soc., v. 61, pp. 379-400.
6. Christensen, W.I., (1979) "Compressional Wave Velocities in Rocks at High Temperature and Pressure, Critical Thermal Gradients, and Crustal Low-Velocity Zones", J. Geophys. Res., v. 84, pp. 6849-6857.
7. Milholland, P., M.H. Mangharani, S.O. Schlanger, and G.H. Sutton, (1980) "Geoacoustic Modeling of Deep-Sea Carbonate Sediments", J. Acoust. Soc. Am., v. 68, n. 5, pp. 1351-1360.
8. Schock, R.N., H. Louis, and E.M. Lilley, (1969) "The Determination of Acoustic Velocities and Dynamic Elastic Moduli in Rocks under Pressure", Lawrence Livermore National Laboratory, UCRL-50750.
9. Berryman, J.G., (1979) "Long-wave Elastic Anisotropy in Transversely Isotropic Media", Geophysics, v. 44, n. 5, pp. 896-917.
10. Melia, P.J. and R.L. Carlson, (1984) "An Experimental Test of P-wave Anisotropy in Stratified Media", Geophysics, v. 49, n. 4, pp. 374-378.
11. Fisher, E.S. and H.J. McSkimin, (1958) "Adiabatic Elastic Moduli of Single Crystal Alpha-Uranium", J. Appl. Physics, v. 29, n. 10, pp. 1473-1484.
12. Alers, G.A., and J.R. Neighbors, (1957) "Crystal Stability and Elastic Constants", J. Appl. Phys., v. 28, n. 12, p. 1514.
13. Brace, W.F., (1964) "Brittle Fracture of Rocks", in State of Stress in the Earth's Crust, W.R. Judd (ed), New York, Elsevier, pp. 11-114.
14. Brace, W.F., (1965) "Some New Measurements of Linear Compressibility of Rocks", J. Geophys. Res., v. 70, pp. 391-398.

15. Simmons, G. and W. F. Brace, (1965) "Comparison of Static and Dynamic Measurements of Compressibility of Rocks", J. Geophys. Res., v. 70, pp. 5649-5656.
16. Heuze, F. E. (1980) "Scale Effects in the Determination of Rock Mass Strength and Deformability", Rock Mechanics, v. 12, pp. 167-192.
17. Thill, R. E. (1983) "Coal and Rock Properties for Pre-mine Planning and Mine Design", in Mine Ground Control, pp. 15-35, U.S. Bureau of Mines, IC 8973.
18. Towse, D. F. and Heuze, F. E. (1983) "Estimating In-Situ Stresses and Rock Mass Properties from Geological and Geophysical Data: Applications in the Hydraulic Fracturing of Tight Gas Reservoirs", Lawrence Livermore National Laboratory, UCRL-53443.
19. Jaeger, J. C. and N. G. W. Cook, (1979) Fundamentals of Rock Mechanics, 3rd Ed., Chapman and Hall, London.

7. ACKNOWLEDGMENTS

This report was prepared by the LLNL Unconventional Gas Program for Morgantown Energy Technology Center, Morgantown, WV, under contract W-7405-ENG-48, with the U.S. Department of Energy.

Discussions with F. E. Heuze and H. Heard throughout this study were very helpful. The author is also indebted to J. Berryman and A. Duba for their comments that substantially improved the manuscript. R. Hill of CER generously furnished the well log tapes. J. Beiriger and S. Trettenero instrumentally prepared the samples. J. Miracle and J. Ricca typed the manuscript. Their contributions are gratefully acknowledged.

APPENDIX A.

Plots of ultrasonic velocities (Figures 2-11) and stiffness coefficients (Figures 12-21) vs. pressure, for Mesaverde sandstones and shales.

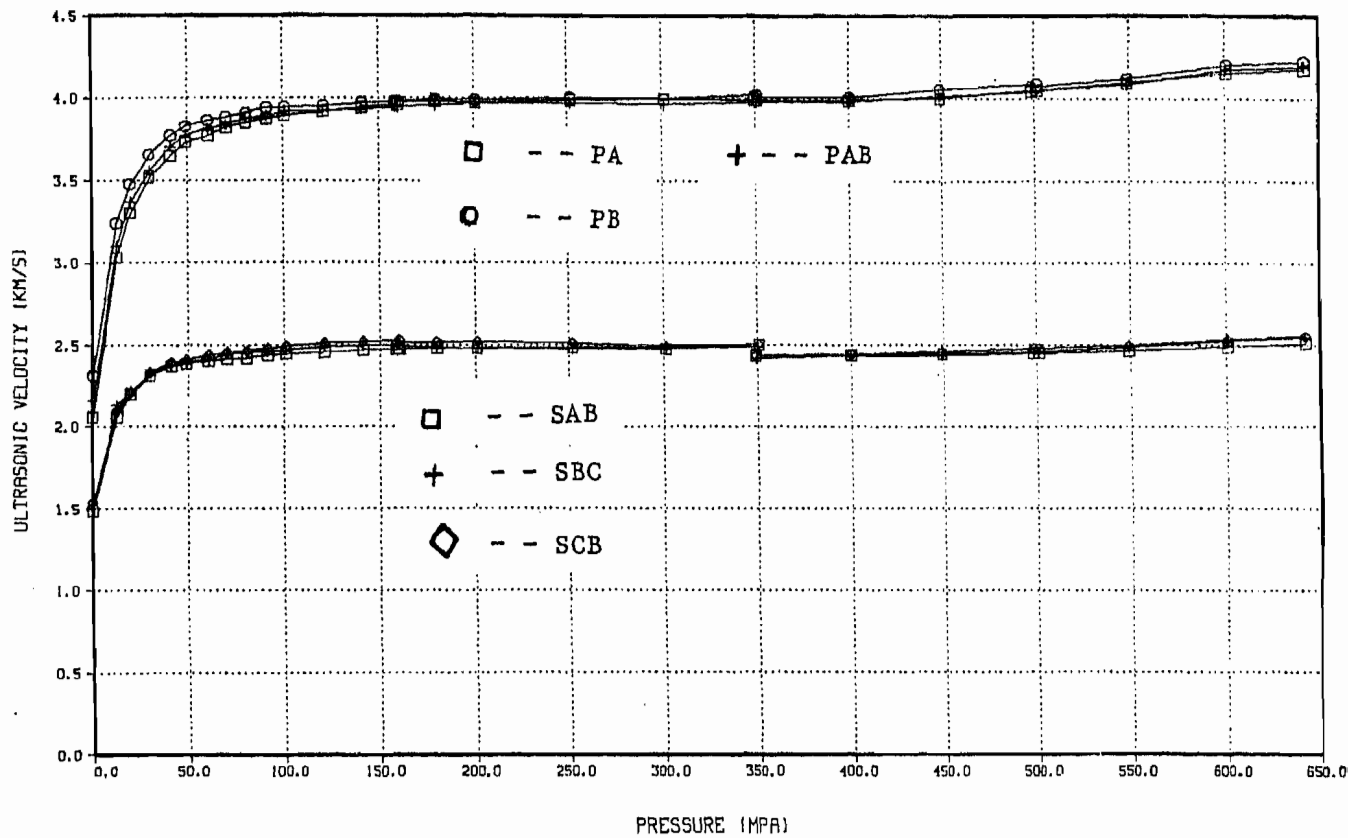


Figure 2. Ultrasonic velocities of Mesaverde sandstone SS1 as a function of pressure. The upper group is P-wave; the lower group is S-wave.

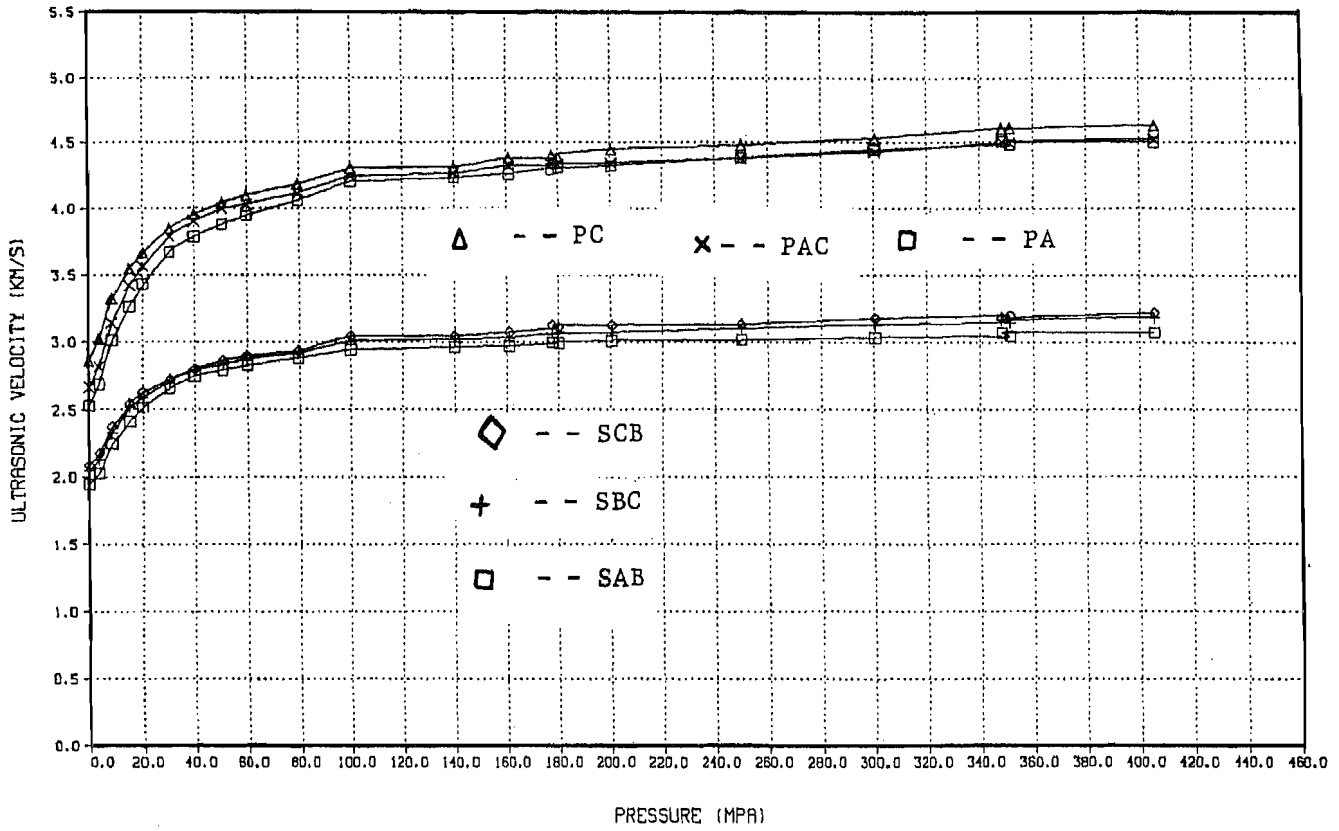


Figure 3. Ultrasonic velocities of Mesaverde shale SH1 as a function of pressure. The upper group is P-wave; the lower group is S-wave.

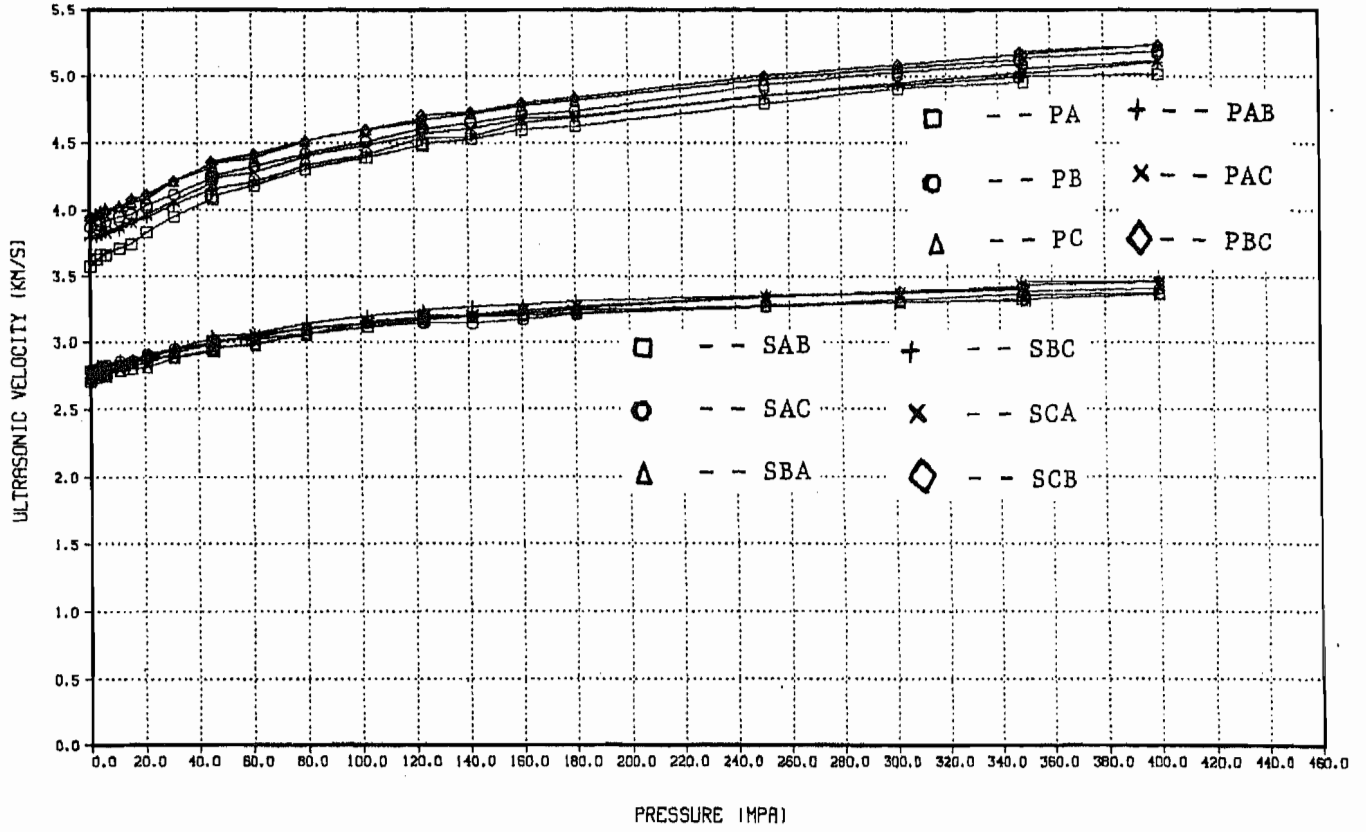


Figure 4. Ultrasonic velocities of Mesaverde Sandstone SS2 as a function of pressure. The upper group is P-wave; the lower group is S-wave.

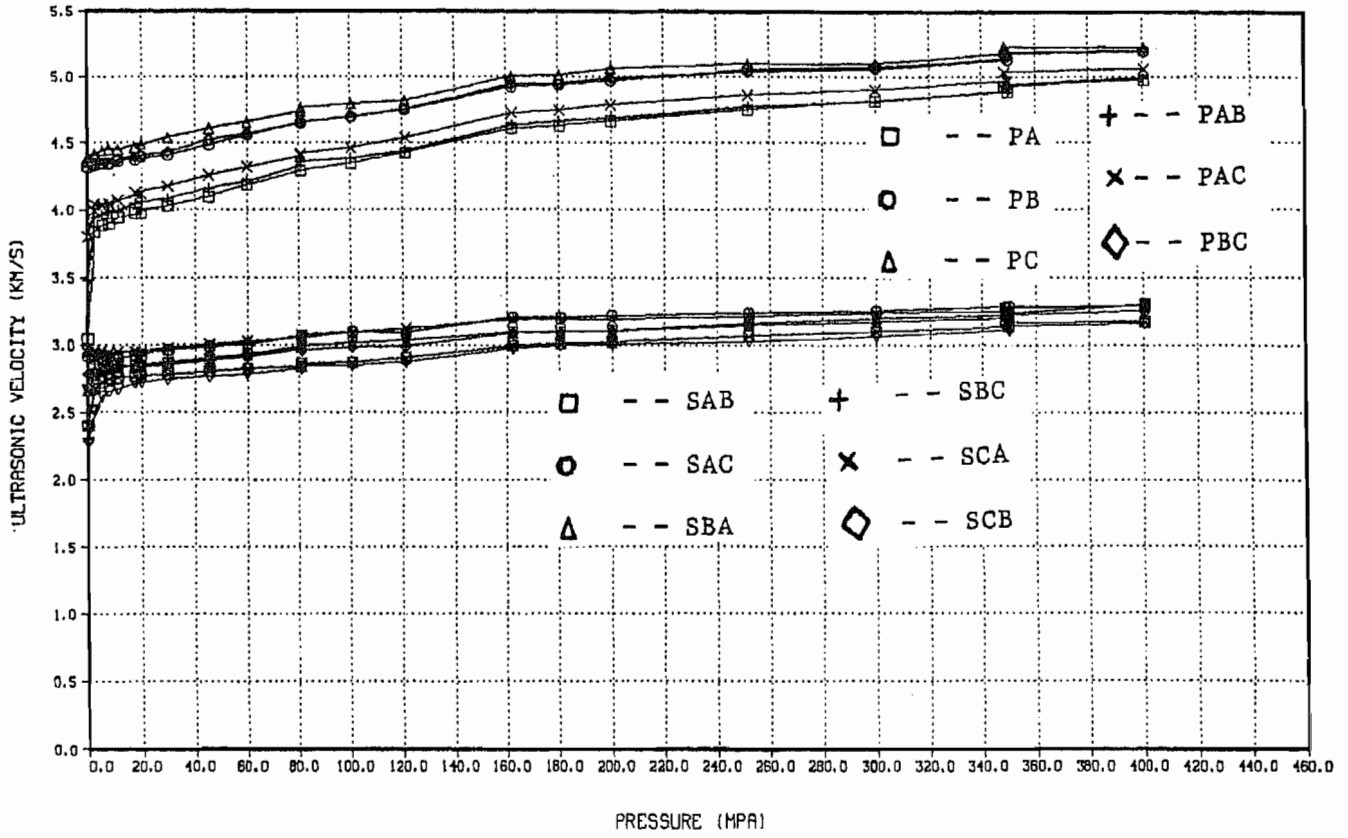


Figure 5. Ultrasonic velocities of Mesaverde shale SH2 as a function of pressure. The upper group is P-wave; the lower group is S-wave.

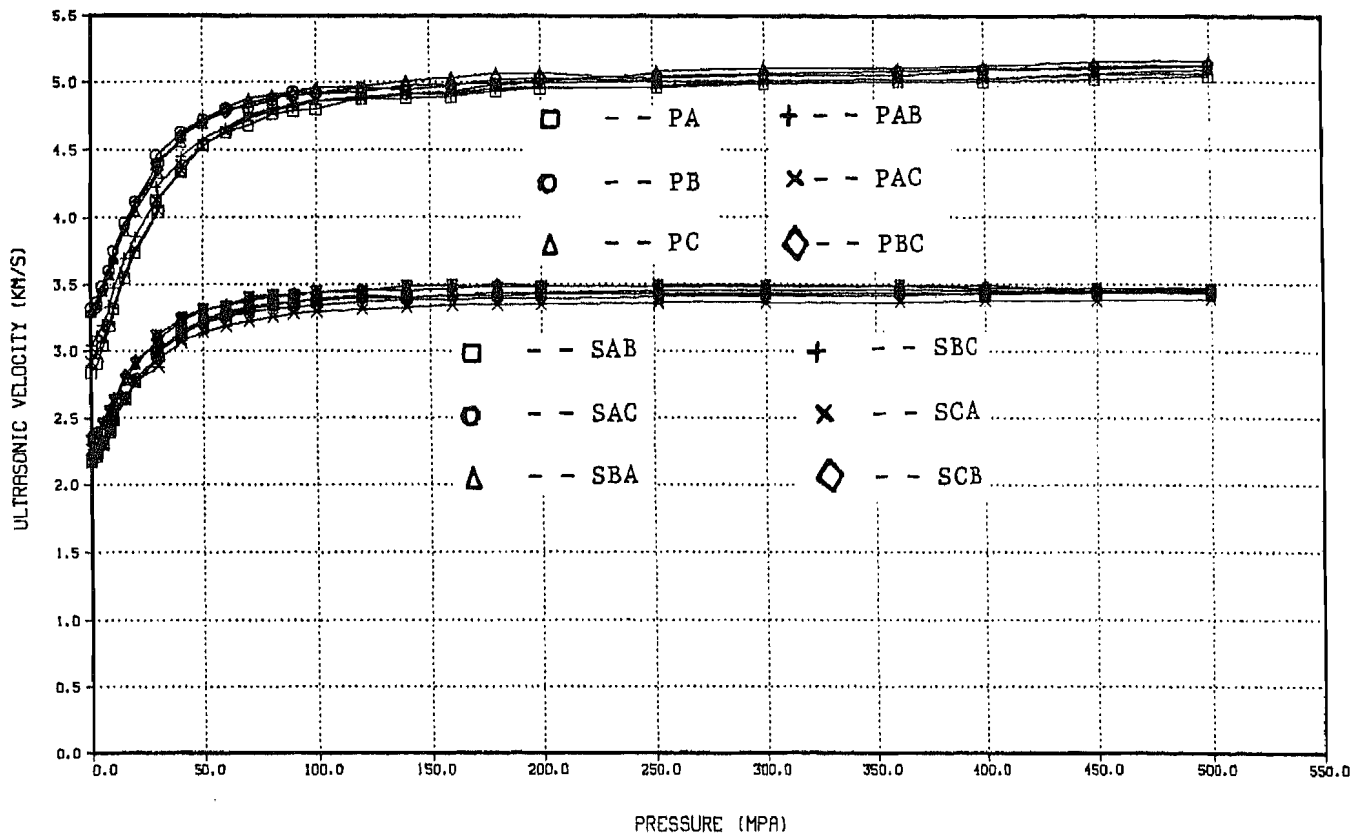


Figure 6. Ultrasonic velocities of Mesaverde sandstone SS3 as a function of pressure. The upper group is P-wave; the lower group is S-wave.

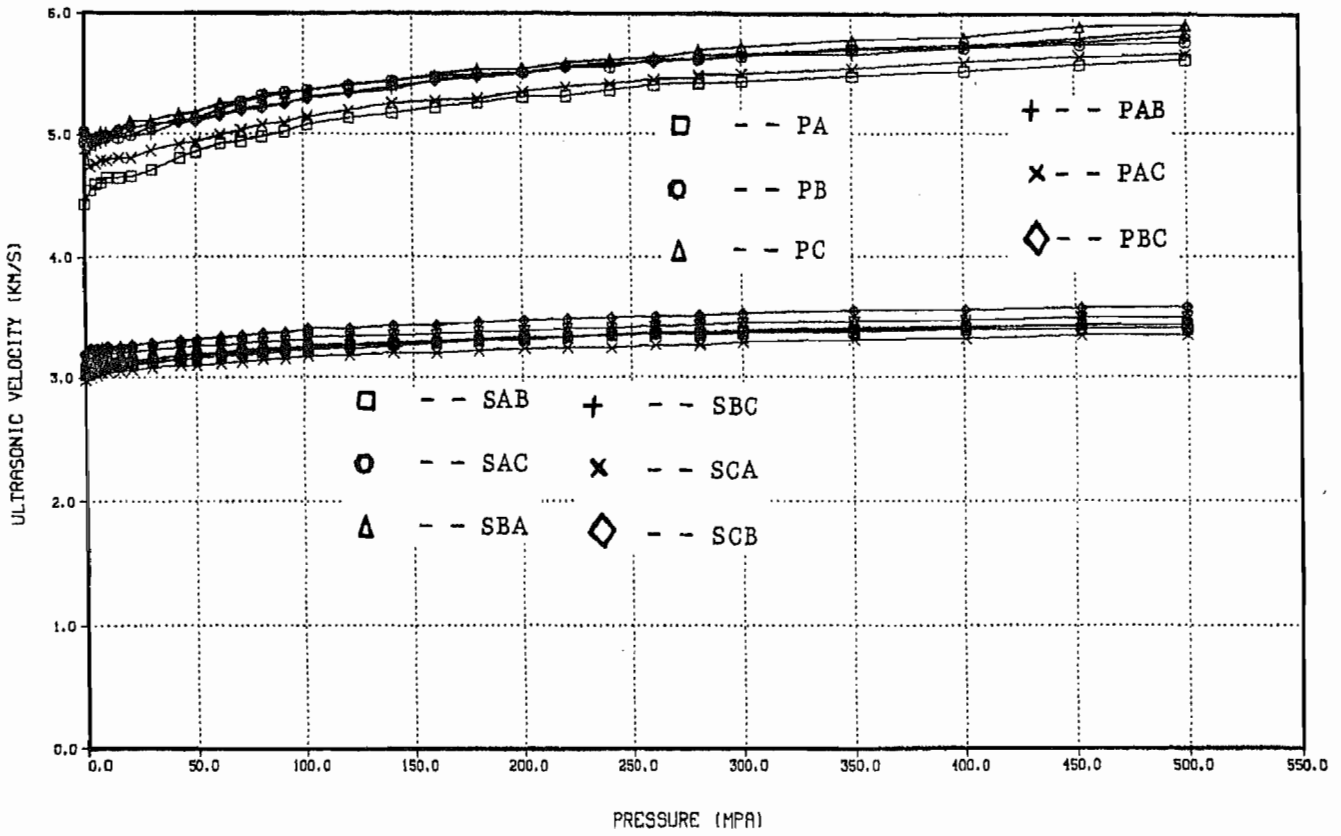


Figure 7. Ultrasonic velocities of Mesaverde shale SH3 as a function of pressure. The upper group is P-wave; the lower group is S-wave.

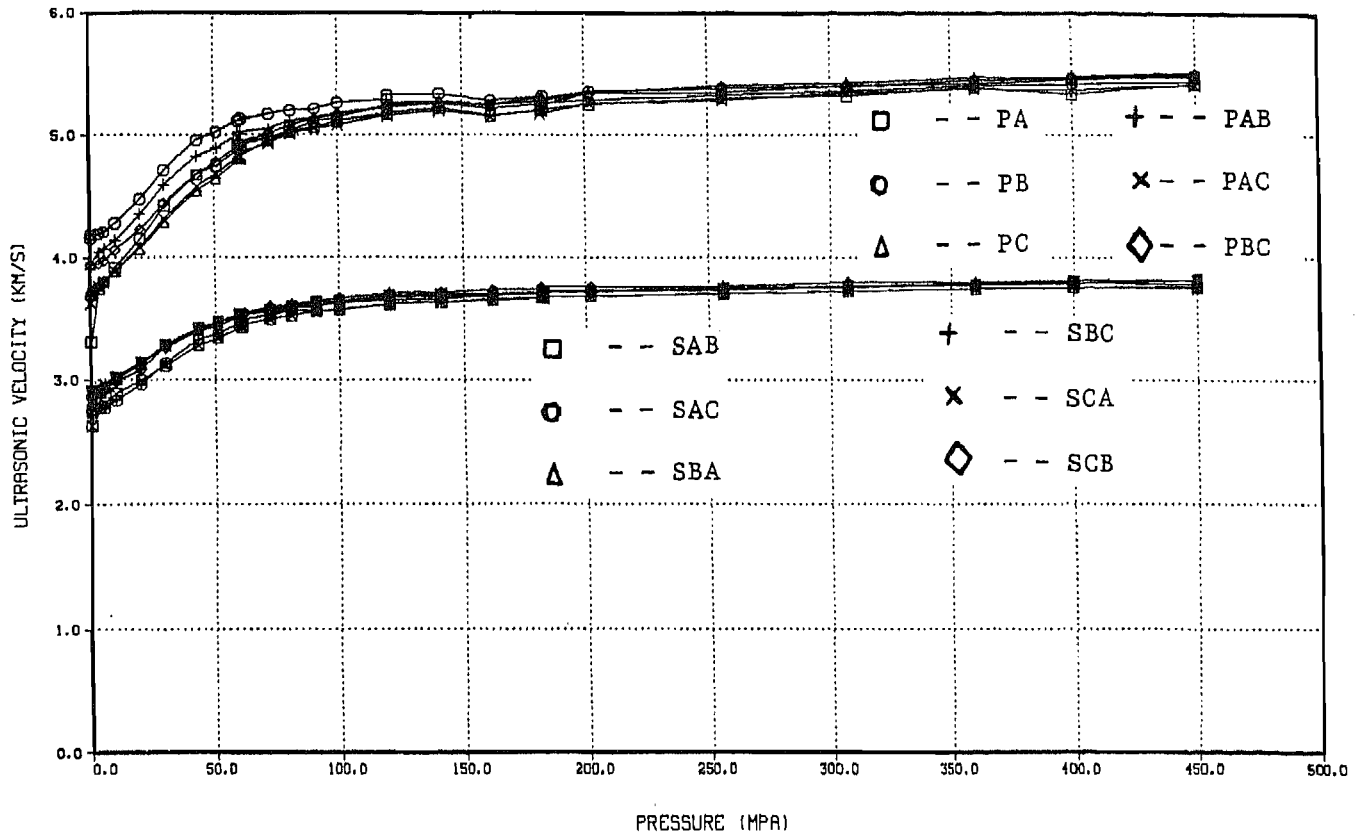


Figure 8. Ultrasonic velocities of Mesaverde sandstone SS4 as a function of pressure. The upper group is P-wave; the lower group is S-wave.

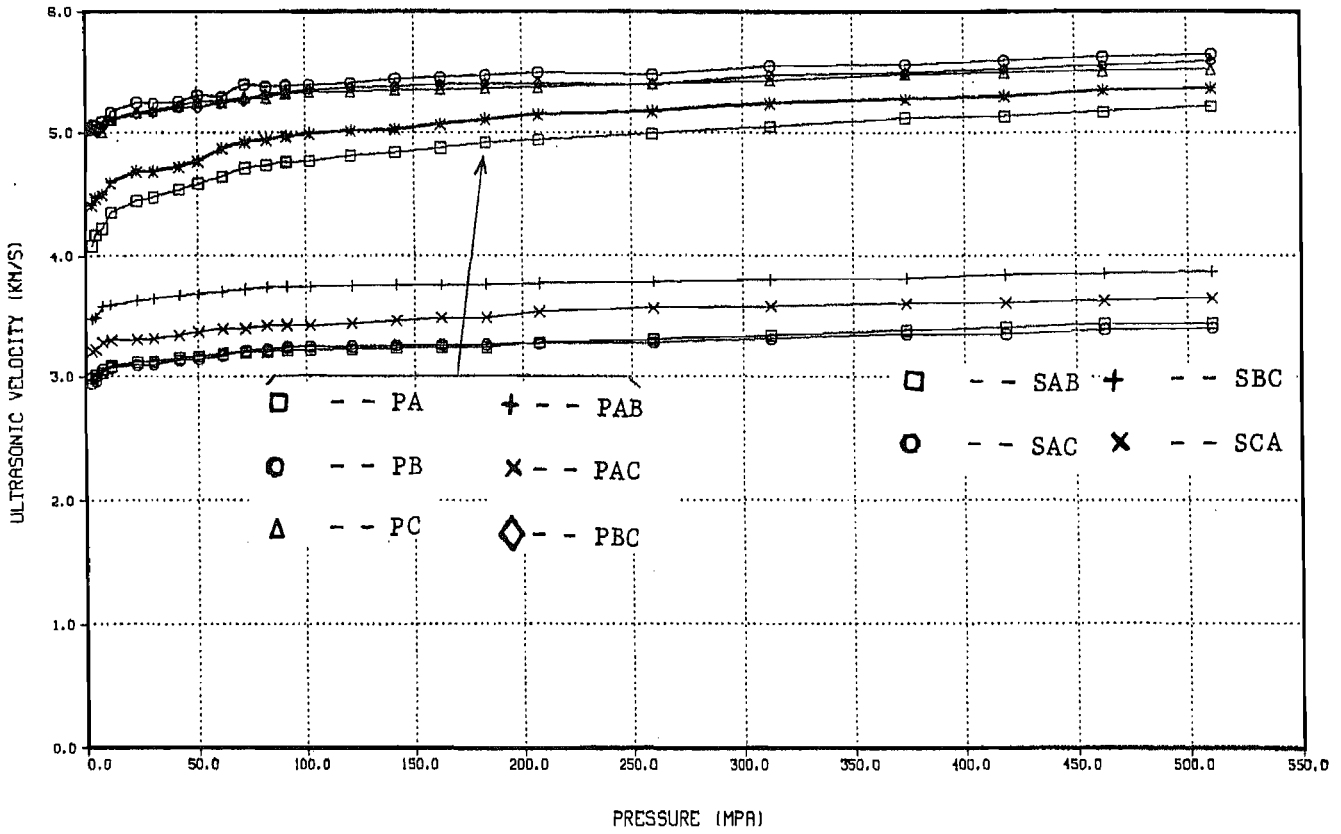


Figure 9. Ultrasonic velocities of Mesaverde shale SH4 as a function of pressure. The upper group is P-wave; the lower group is S-wave.

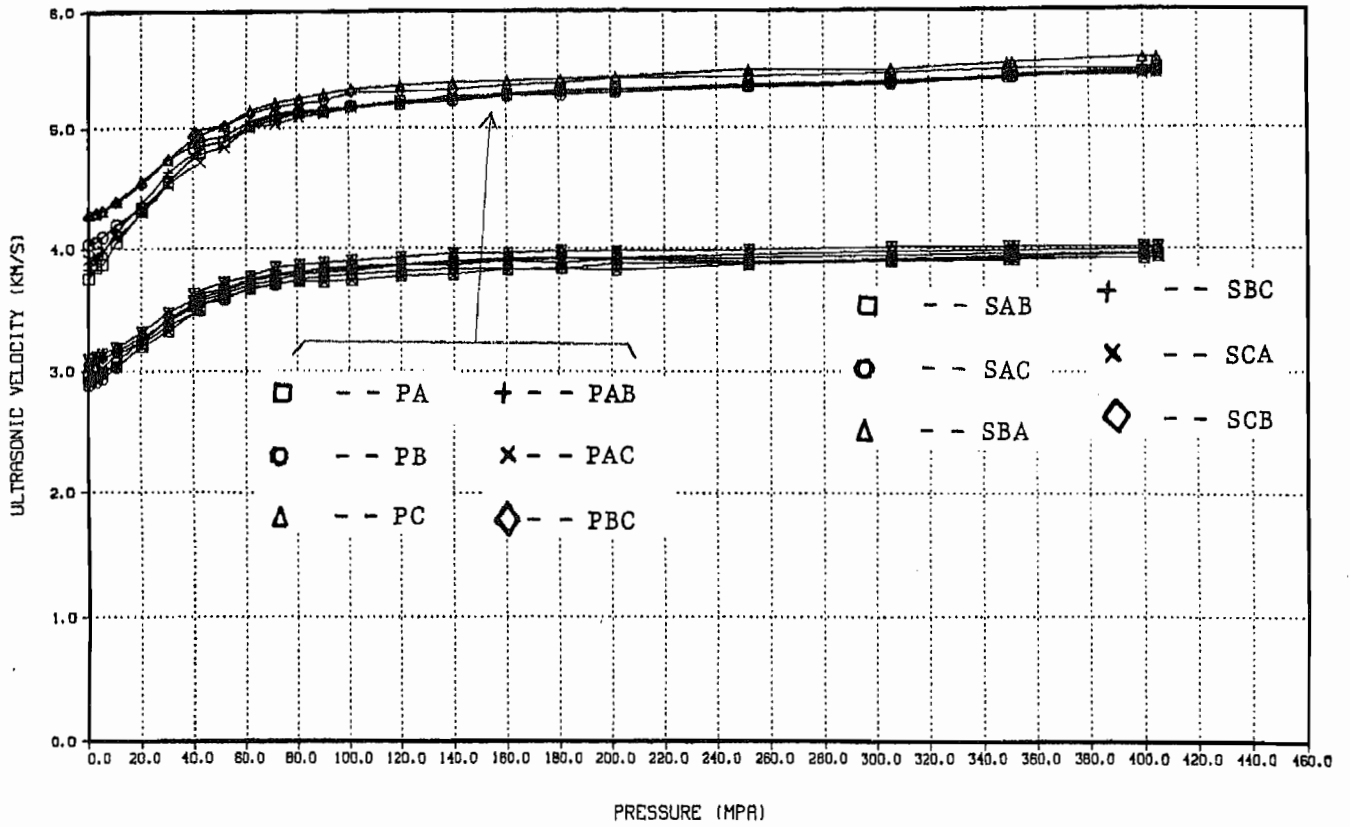


Figure 10. Ultrasonic velocities of Mesaverde sandstone SS5 as a function of pressure. The upper group is P-wave; the lower group is S-wave.

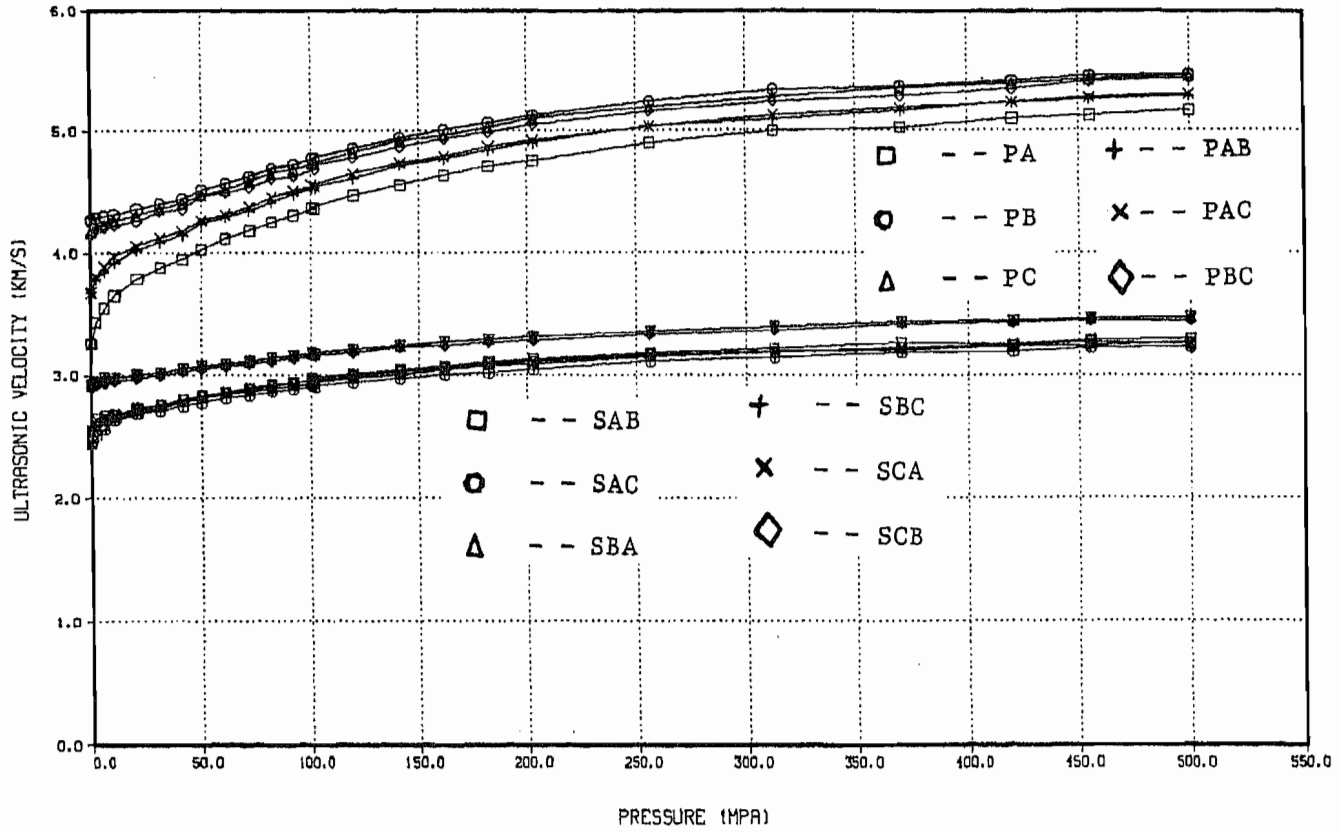


Figure 11. Ultrasonic velocities of Mesaverde shale SH5 as a function of pressure. The upper group is P-wave; the lower group is S-wave.

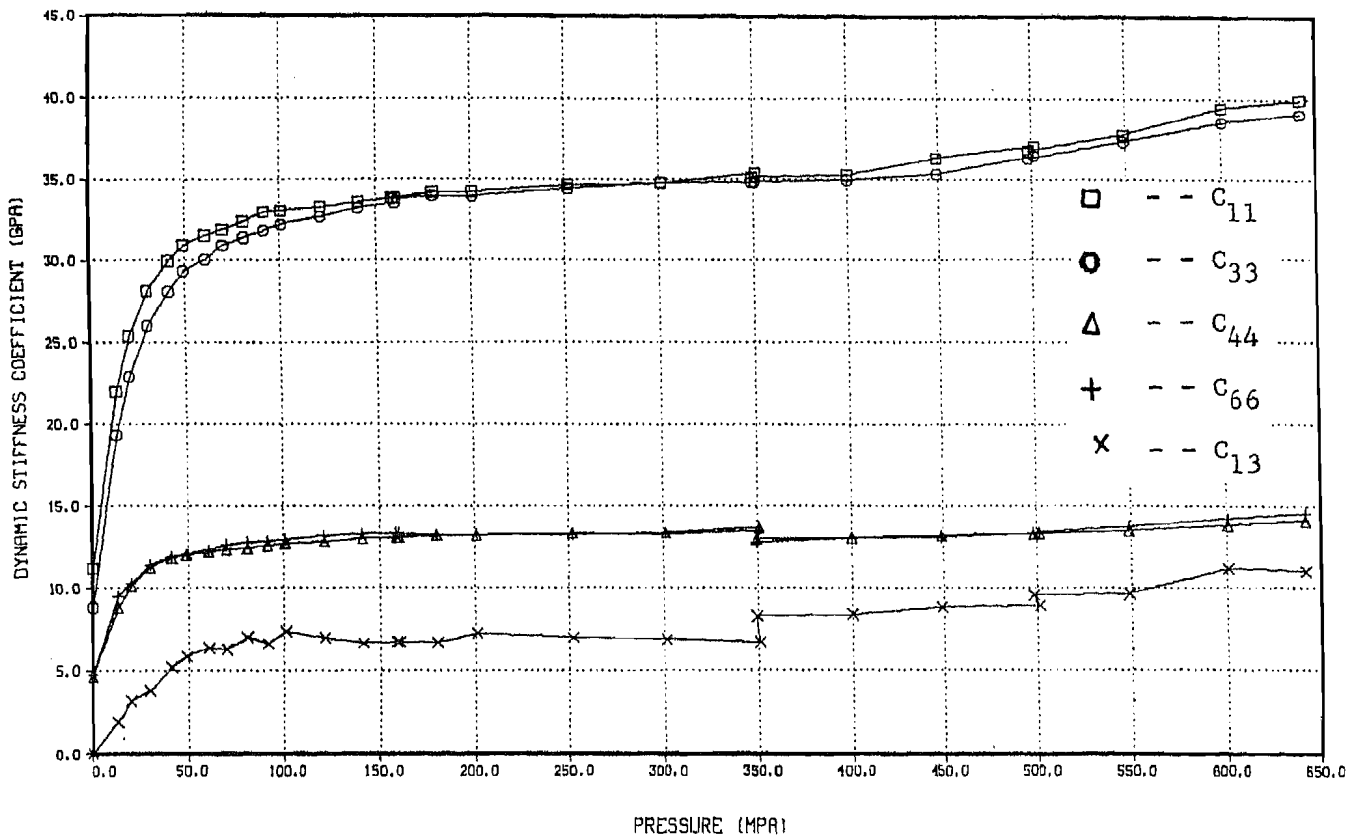


Figure 12. Dynamic stiffness coefficients of Mesaverde sandstone SS1 as a function of pressure.

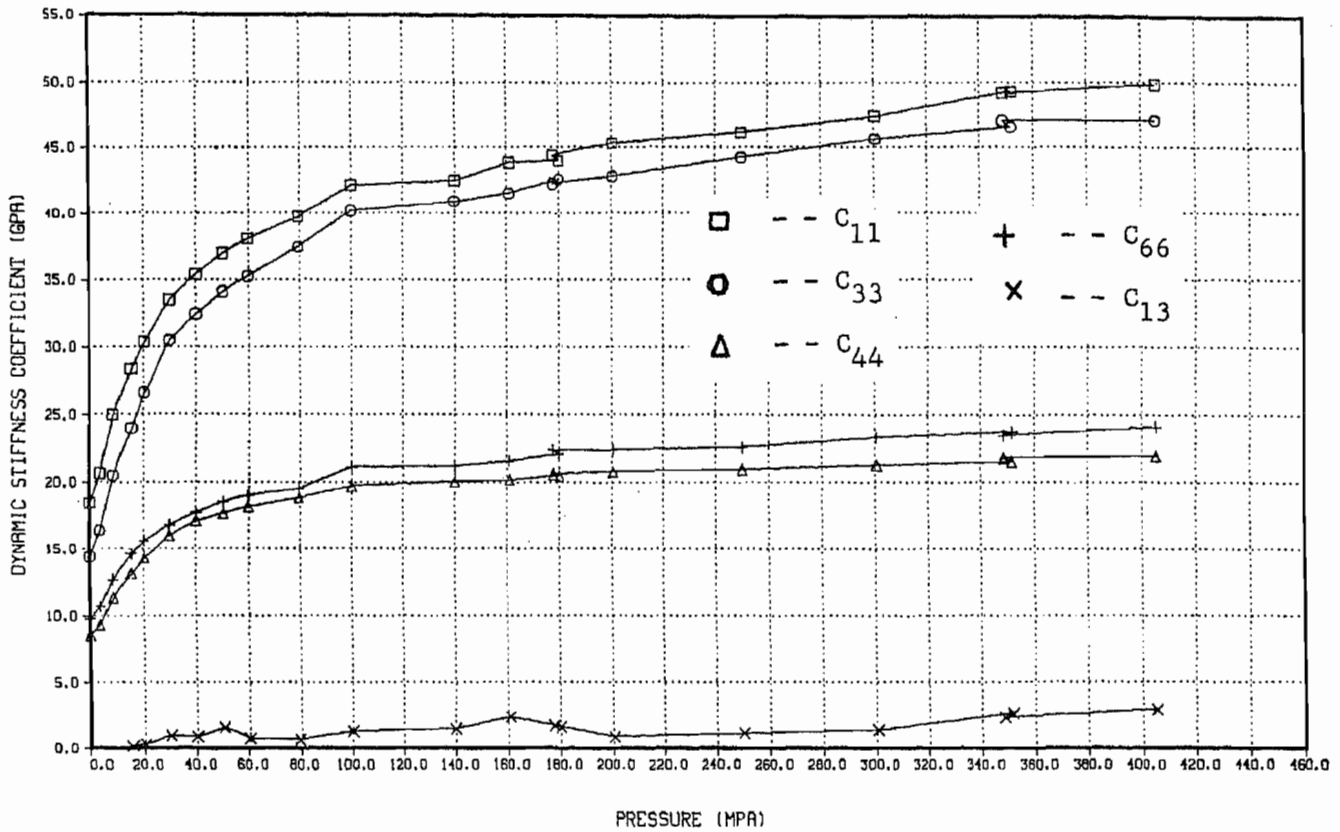


Figure 13. Dynamic stiffness coefficients of Mesaverde shale SH1 as a function of pressure.

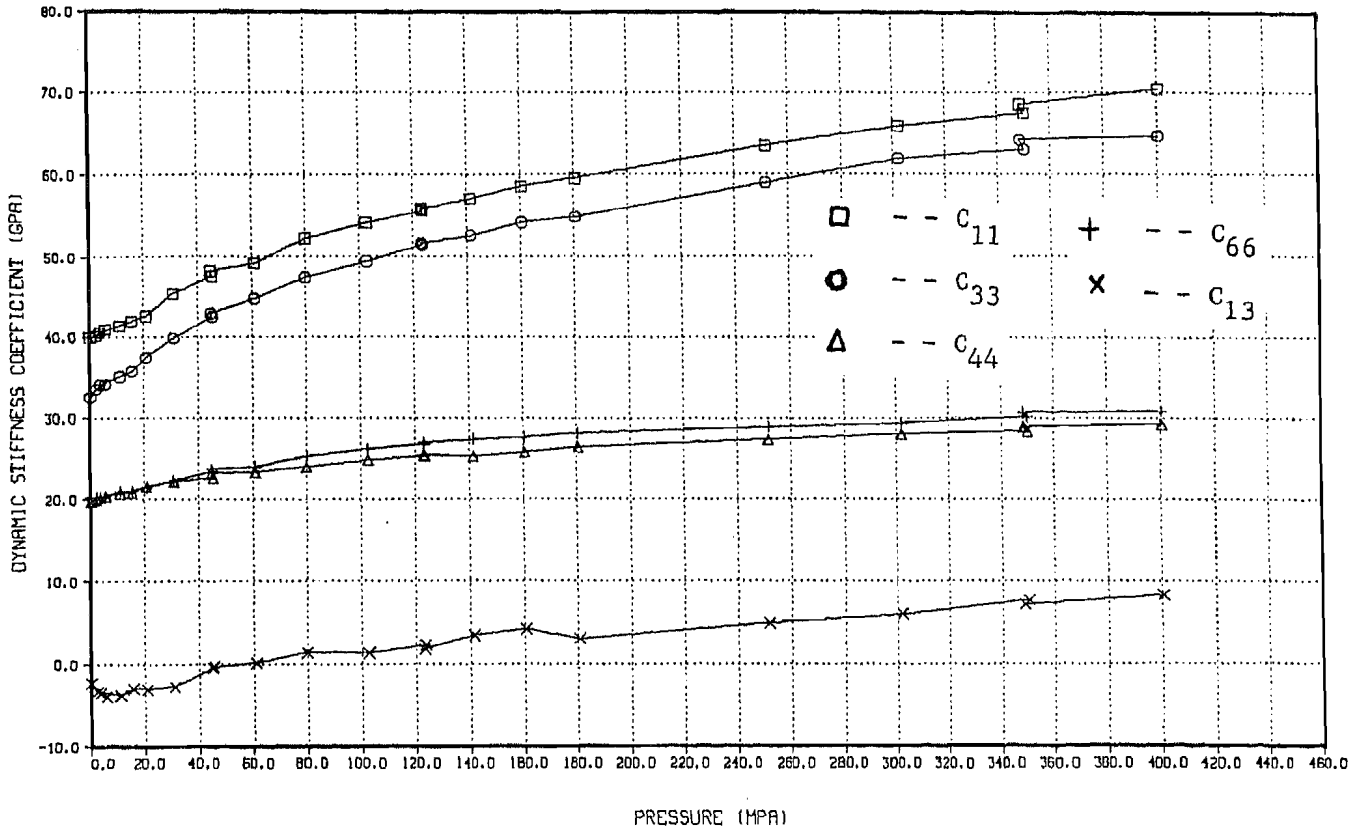


Figure 14. Dynamic stiffness coefficients of Mesaverde sandstone SS2 as a function of pressure.

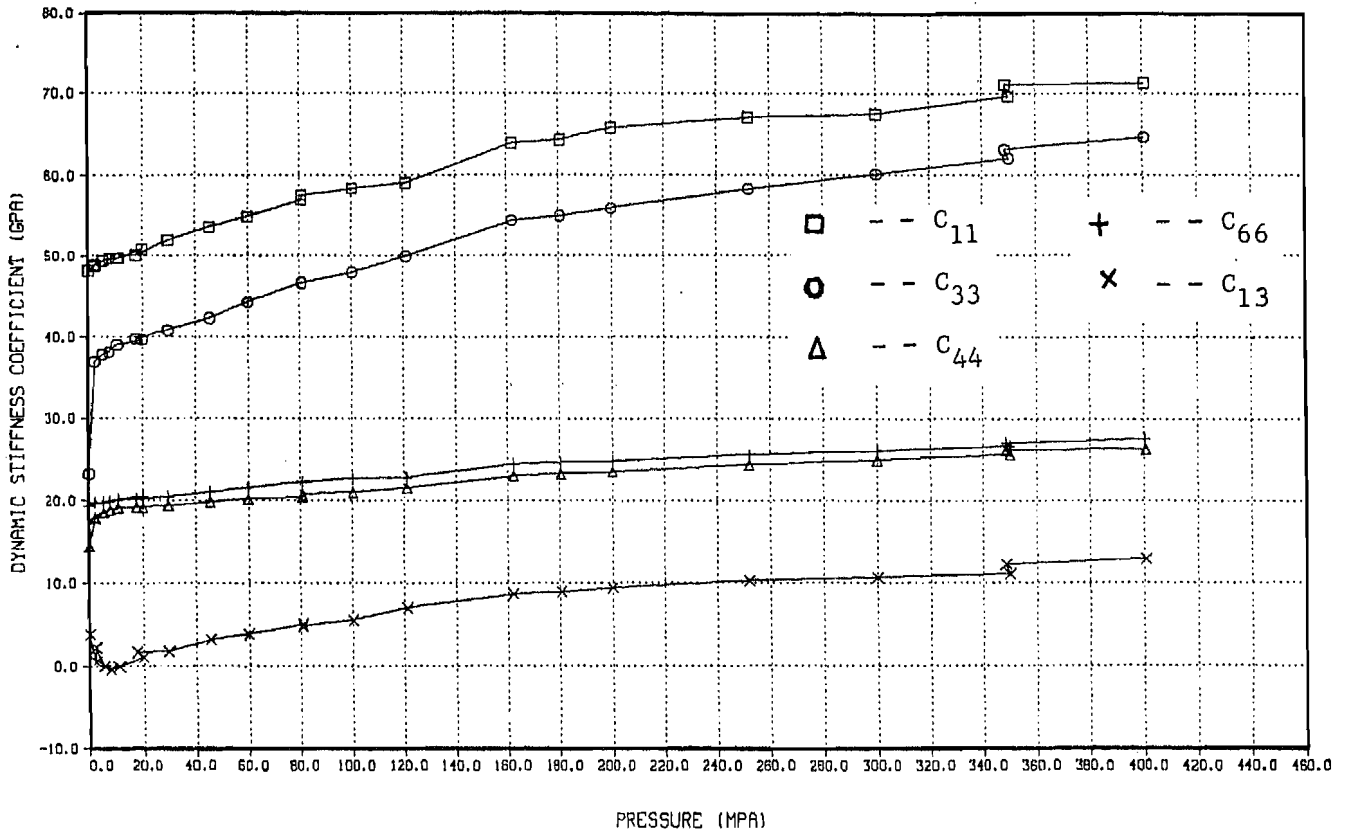


Figure 15. Dynamic stiffness coefficients of Mesaverde shale SH2 as a function of pressure.

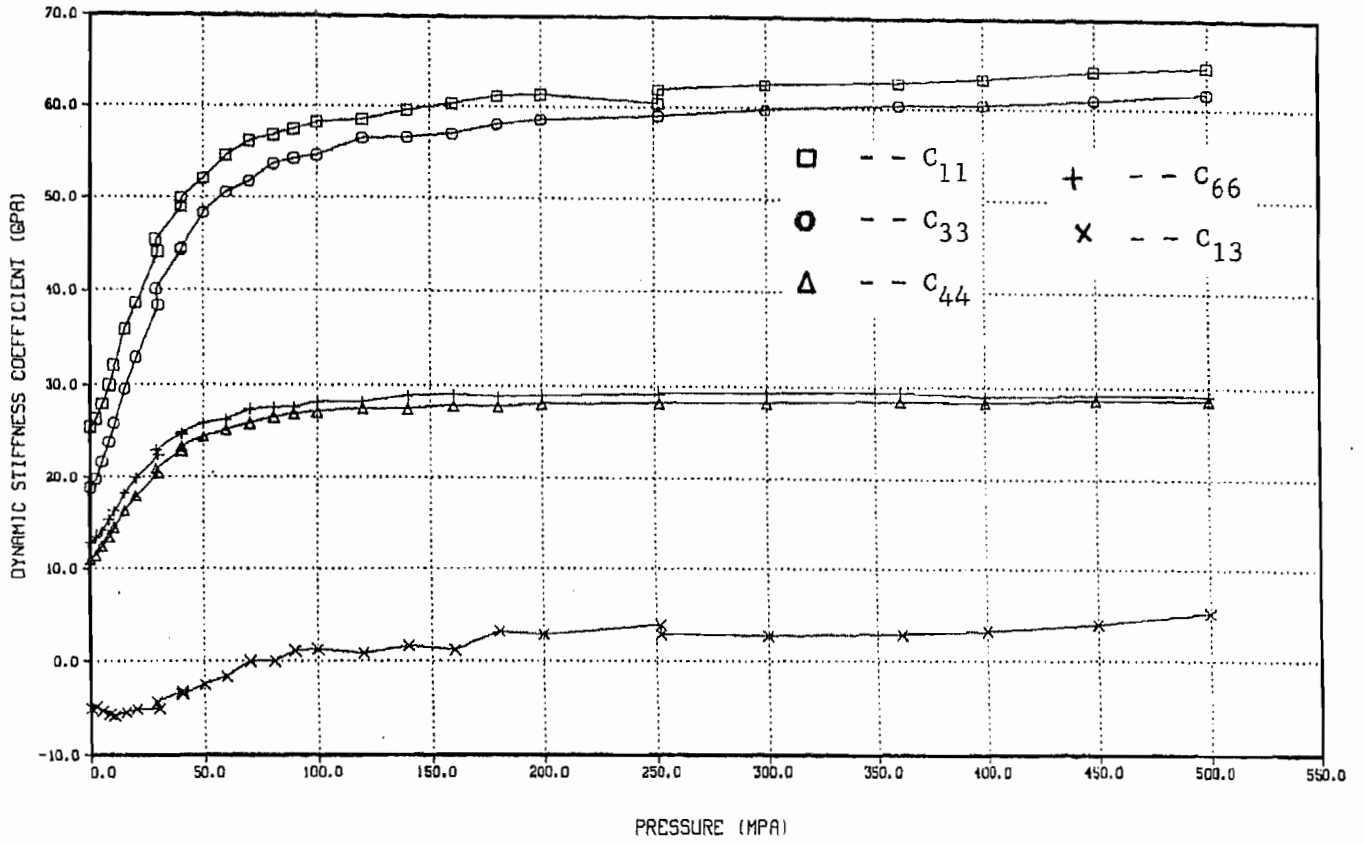


Figure 16. Dynamic stiffness coefficients of Mesaverde sandstone SS3 as a function of pressure.

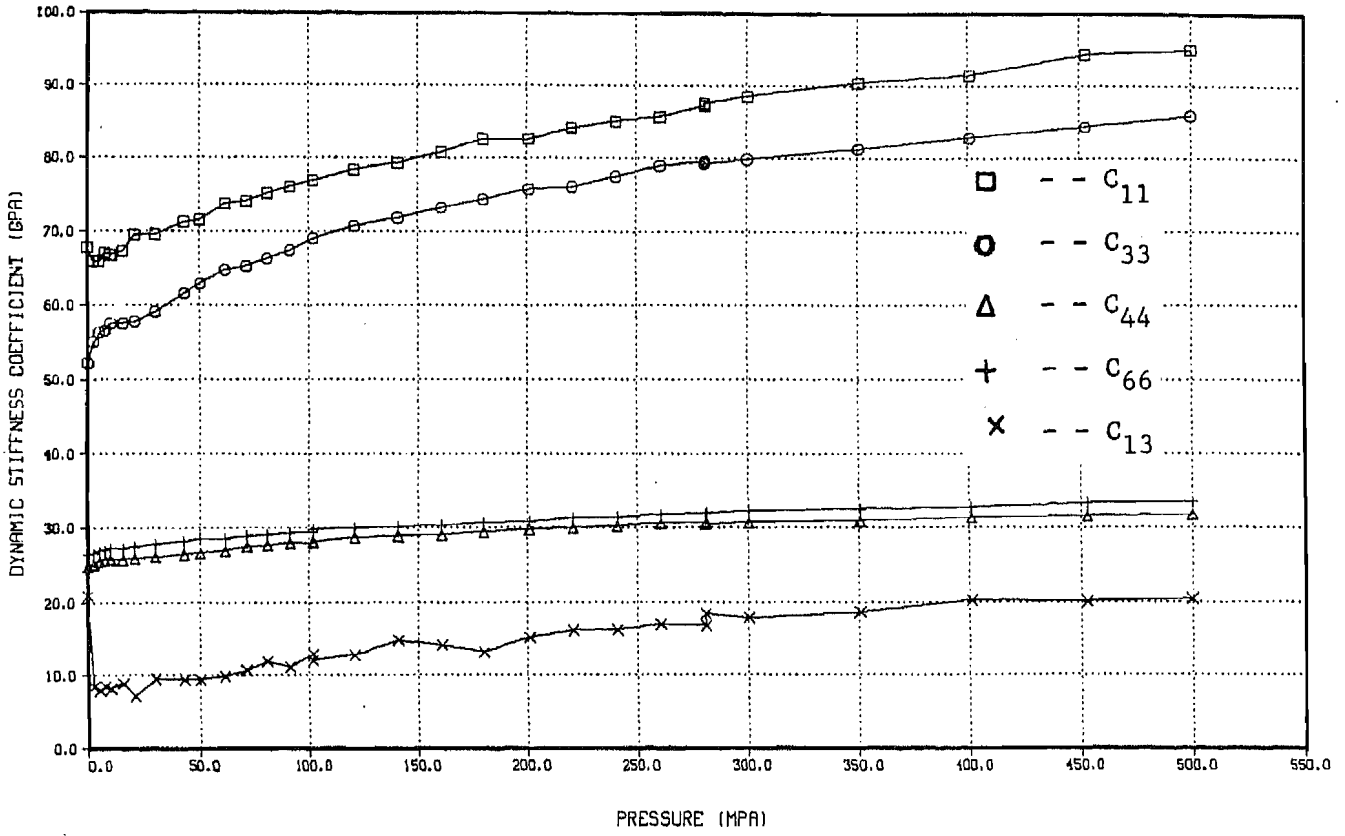


Figure 17. Dynamic stiffness coefficients of Mesaverde sandstone SH3 as a function of pressure.

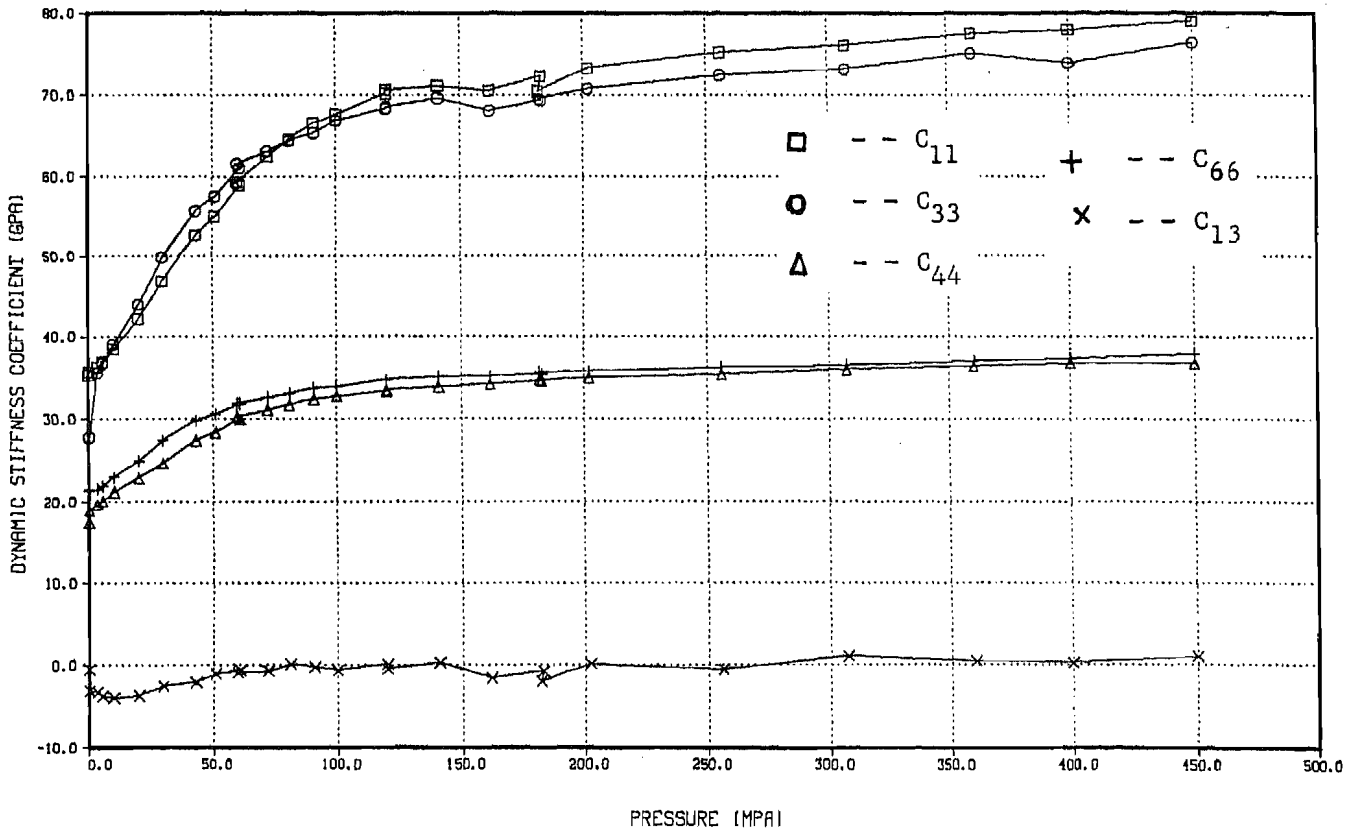


Figure 18. Dynamic stiffness coefficients of Mesaverde sandstone SS4 as a function of pressure.

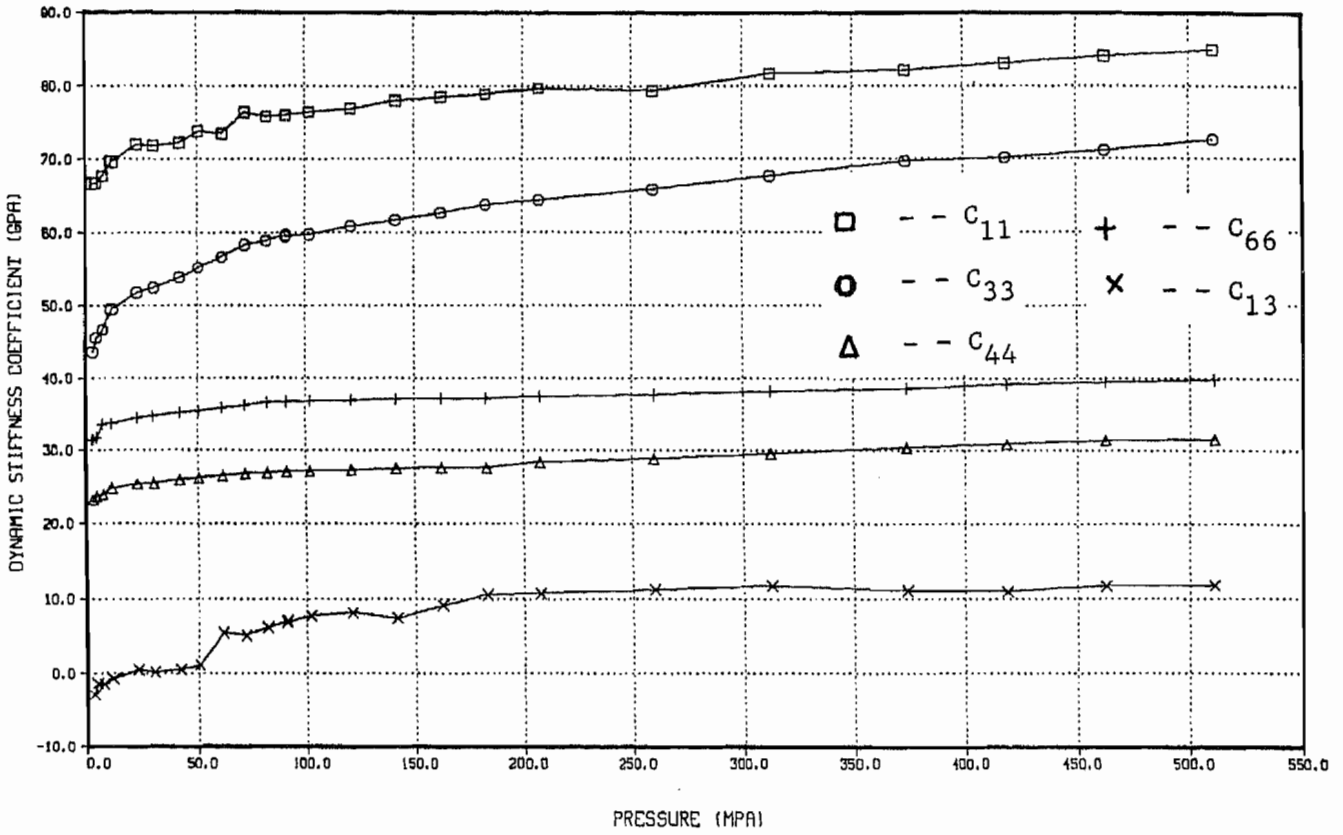


Figure 19. Dynamic stiffness coefficients of Mesaverde shale SH4 as a function of pressure.

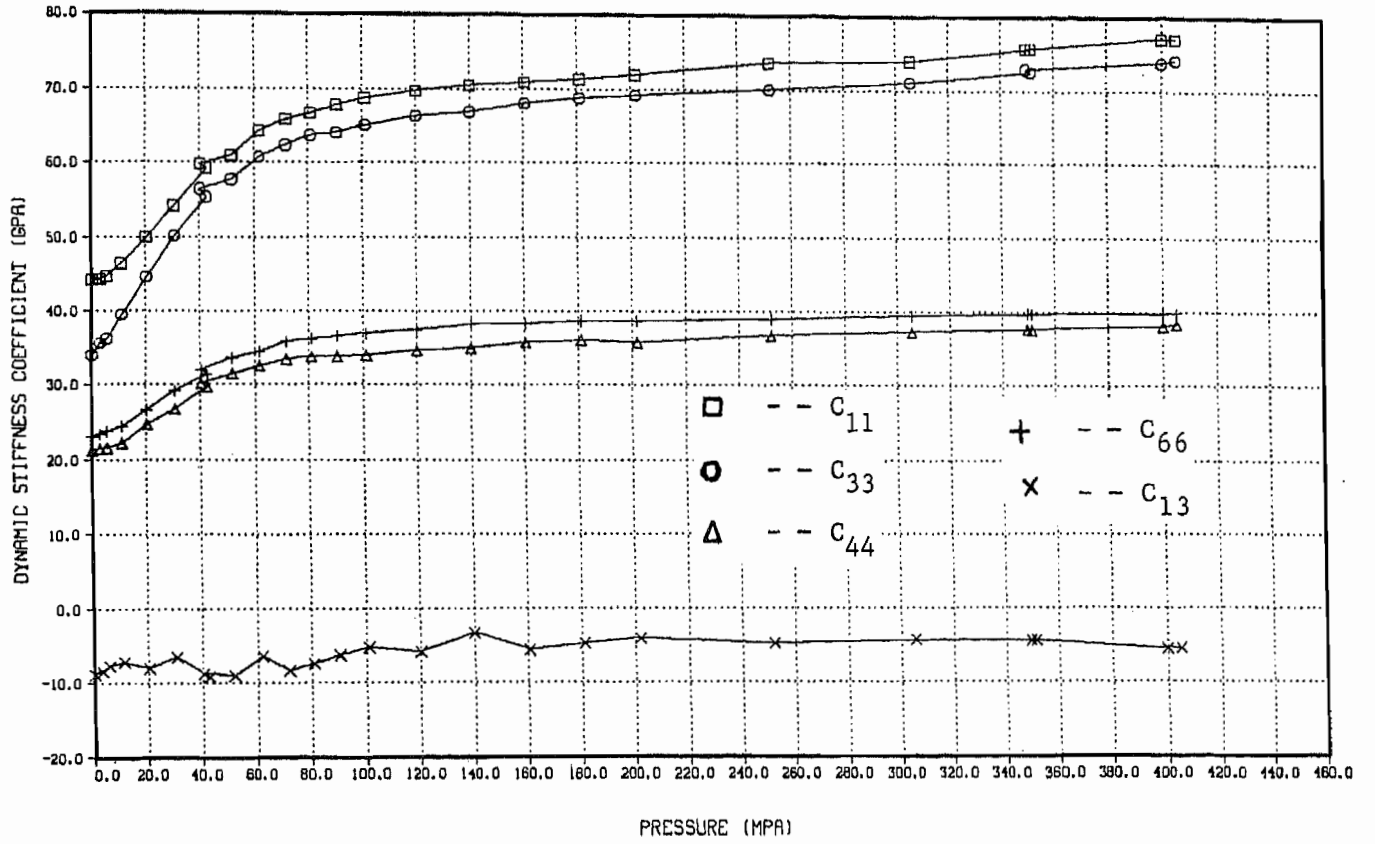


Figure 20. Dynamic stiffness coefficients of Mesaverde sandstone SS5 as a function of pressure.

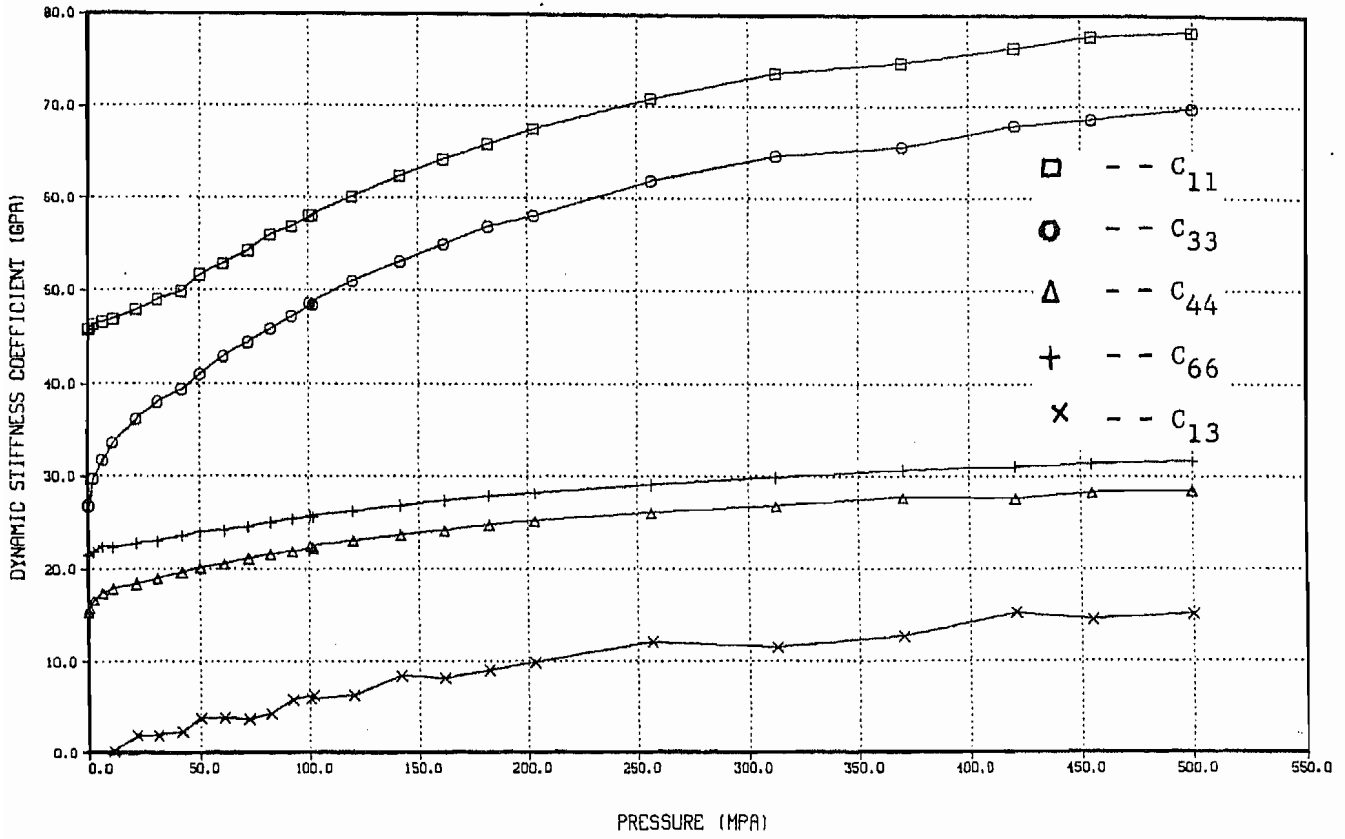


Figure 21. Dynamic stiffness coefficients of Mesaverde shale SH5 as a function of pressure.

APPENDIX B.

Plots of in situ P-wave velocity and laboratory determined P-wave velocity vs depth for Mesaverde rocks (Figures 22-25).

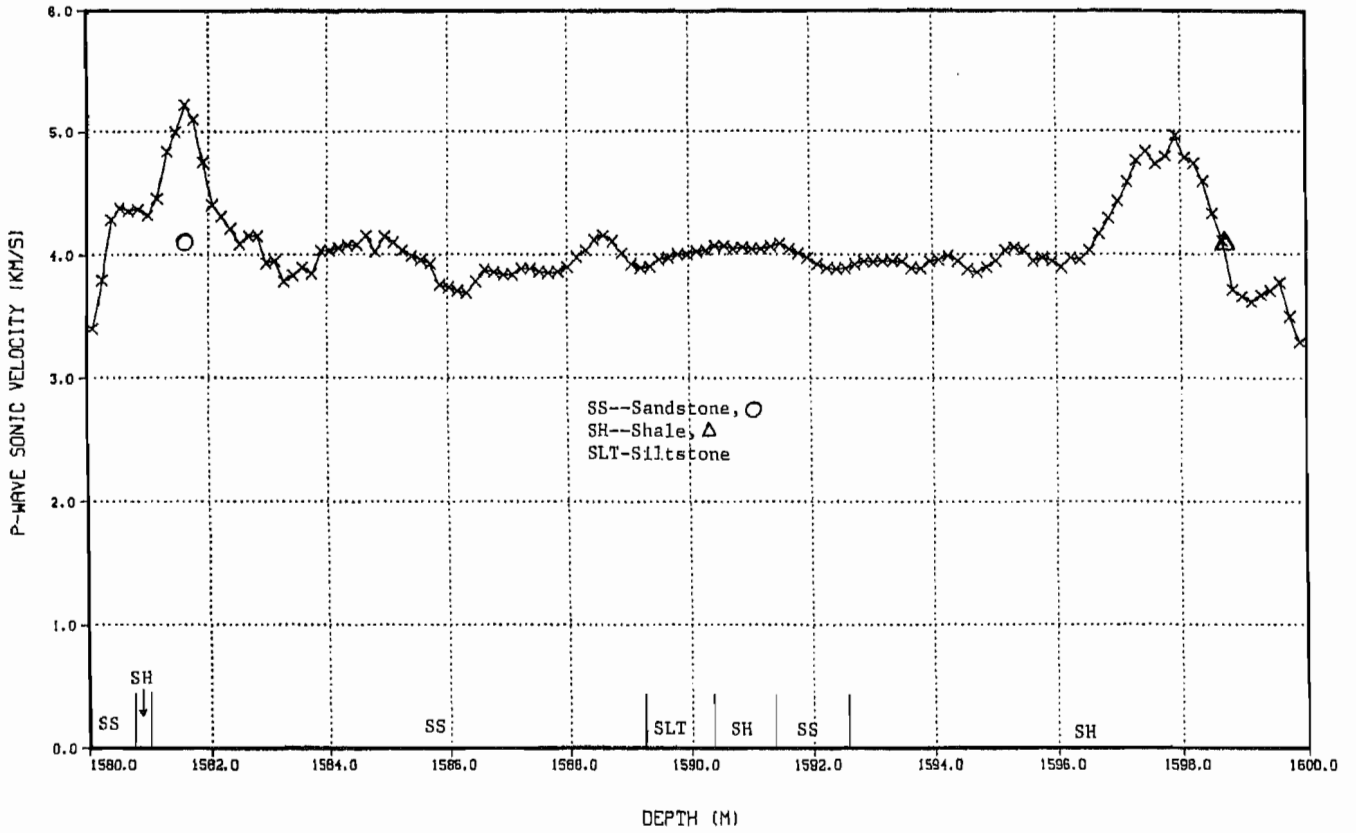


Figure 22. P-wave velocity as function of depth and rock types of PTS24-19 well. ○ and △ are the laboratory measured P-wave velocity of sandstone and shale respectively.

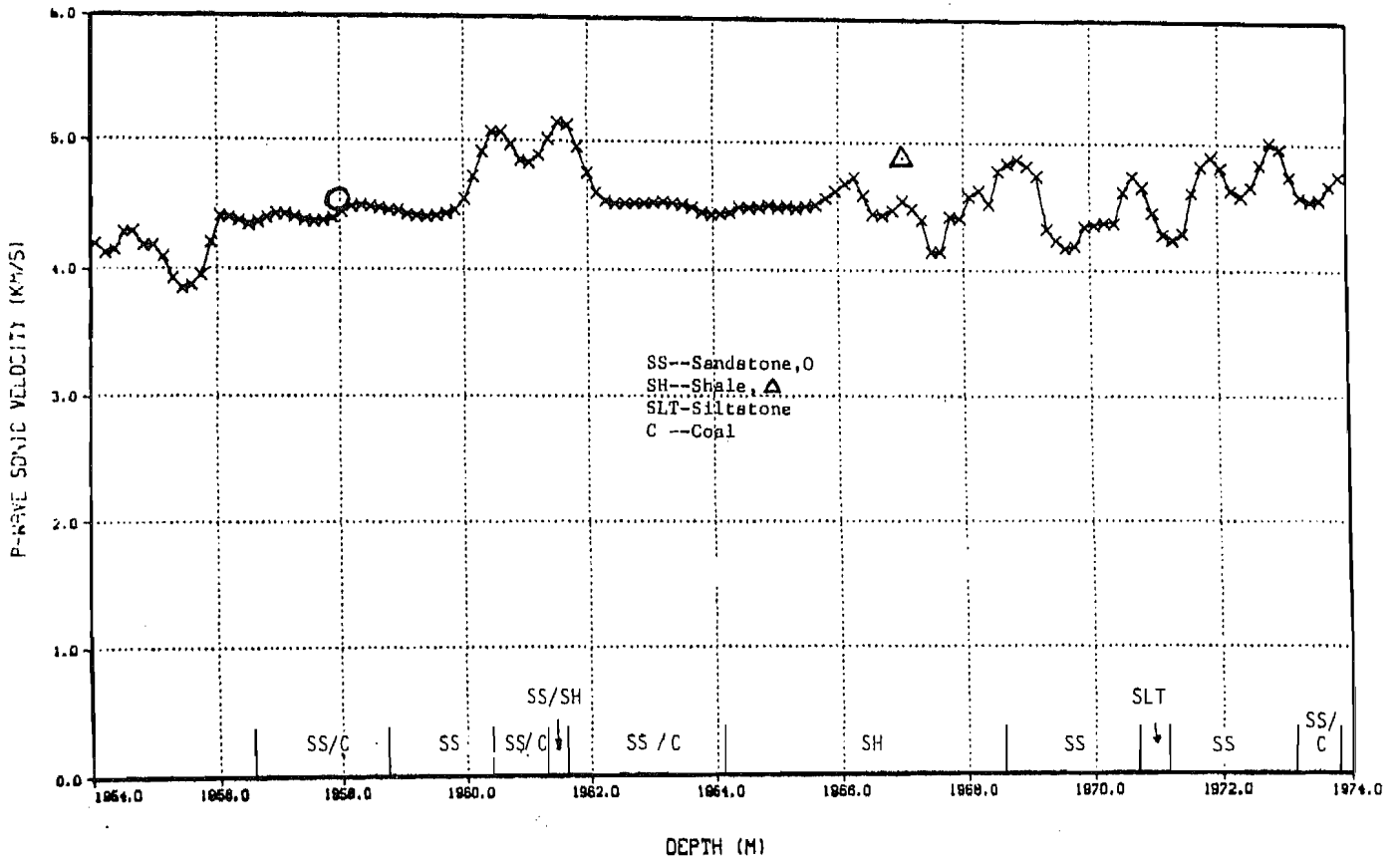


Figure 23. P-wave velocity as functions of depth and rock types of PTS 22-12 well. O and Δ are the laboratory measured P-wave velocity of sandstone and shale respectively.

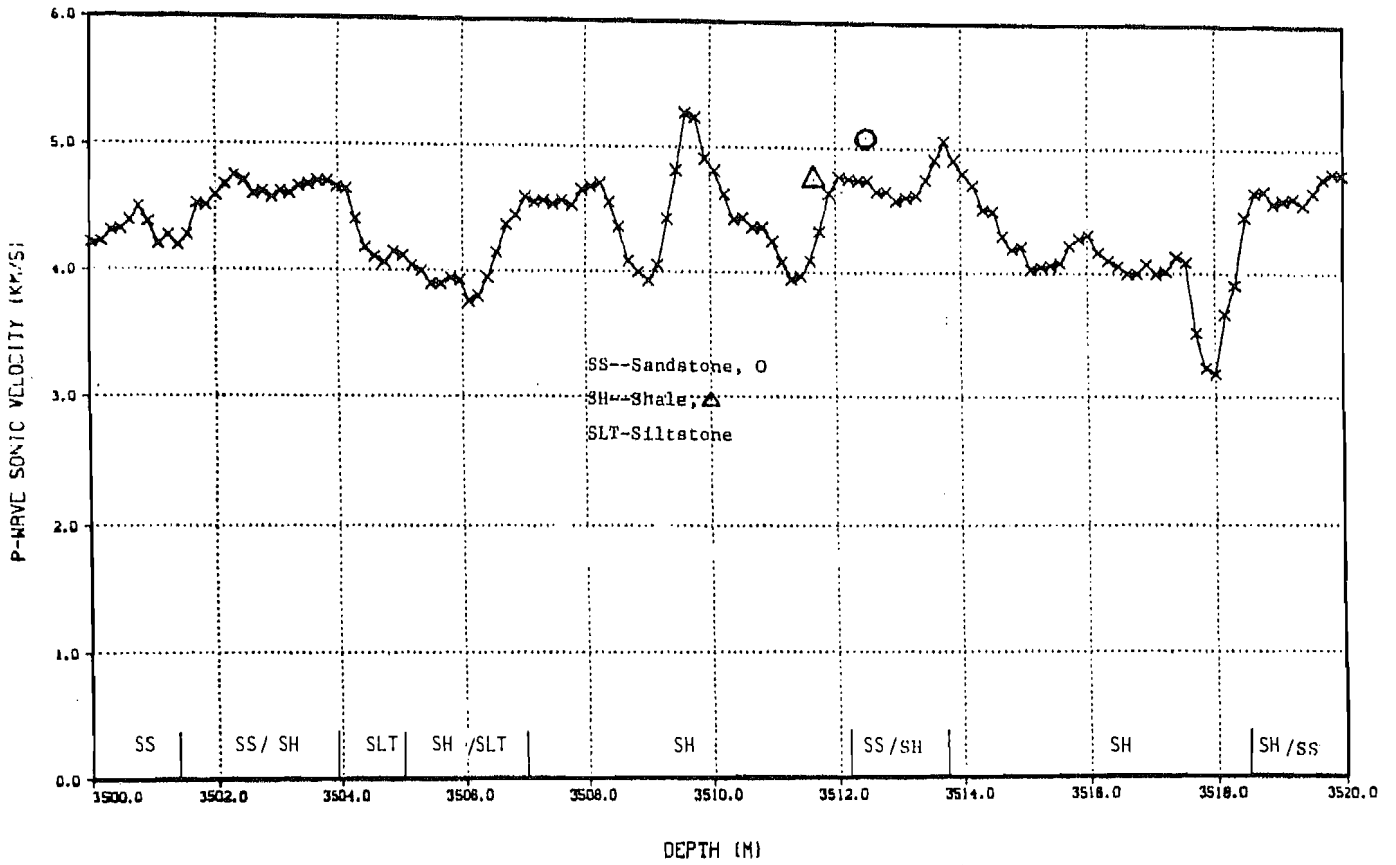


Figure 24. P-wave velocity as function of depth and rock types of PTS 3-10A well. O and Δ are the laboratory measured P-wave velocity of sandstone and shale respectively.

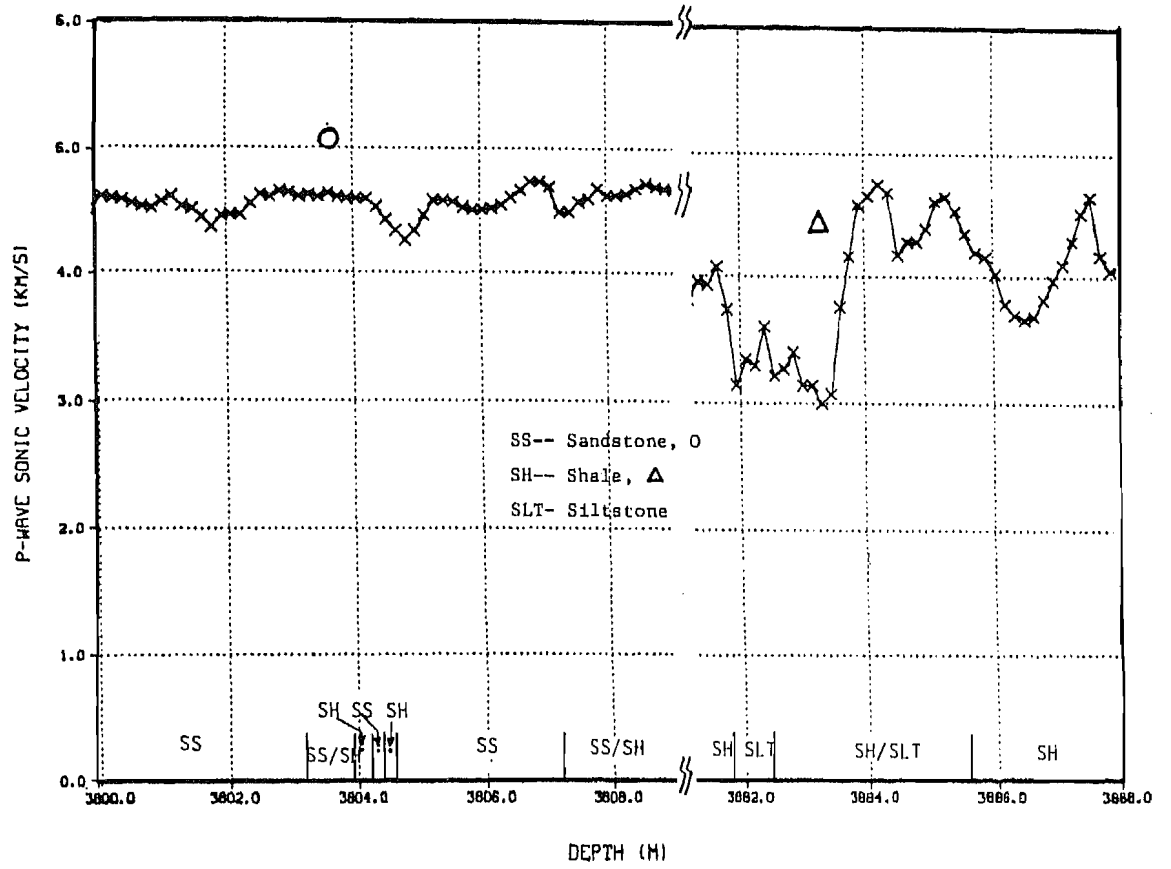


Figure 25. P-wave velocity as function of depth and rock types of Rainbow Resource 1-3 well. O and Δ are the laboratory measured P-wave velocity of sandstone and shale respectively.